NAVAL POSTGRADUATE SCHOOL

MONTEREY, CALIFORNIA

THESIS

AN IMPROVED RECTENNA FOR WIRELESS POWER TRANSMISSION FOR UNMANNED AIR VEHICLES

by

Chun-Yi Liu

September 2011

Thesis Advisor: David C. Jenn
Second Reader: Ric Romero

Approved for public release; distribution is unlimited

THIS PAGE INTENTIONALLY LEFT BLANK

REPORT DOCUMENTATION PAGE		*Form Approved OMB No. 0704-0188*
Public reporting burden for this collection of information is estimated to average 1 hour per response, including the time for reviewing instruction, searching existing data sources, gathering and maintaining the data needed, and completing and reviewing the collection of information. Send comments regarding this burden estimate or any other aspect of this collection of information, including suggestions for reducing this burden, to Washington headquarters Services, Directorate for Information Operations and Reports, 1215 Jefferson Davis Highway, Suite 1204, Arlington, VA 22202-4302, and to the Office of Management and Budget, Paperwork Reduction Project (0704-0188) Washington DC 20503.		
1. AGENCY USE ONLY *(Leave blank)*	**2. REPORT DATE** September 2011	**3. REPORT TYPE AND DATES COVERED** Master's Thesis
4. TITLE AND SUBTITLE An Improved Rectenna for Wireless Power Transmission for Unmanned Air Vehicles		**5. FUNDING NUMBERS**
6. AUTHOR(S) Chun-Yi Liu		
7. PERFORMING ORGANIZATION NAME(S) AND ADDRESS(ES) Naval Postgraduate School Monterey, CA 93943-5000		**8. PERFORMING ORGANIZATION REPORT NUMBER**
9. SPONSORING /MONITORING AGENCY NAME(S) AND ADDRESS(ES) N/A		**10. SPONSORING/MONITORING AGENCY REPORT NUMBER**
11. SUPPLEMENTARY NOTES The views expressed in this thesis are those of the author and do not reflect the official policy or position of the Department of Defense or the U.S. Government. IRB Protocol number NA.		
12a. DISTRIBUTION / AVAILABILITY STATEMENT Approved for public release; distribution is unlimited		**12b. DISTRIBUTION CODE** A

13. ABSTRACT (maximum 200 words)

This thesis continues an NPS project related to wireless power transmission for micro air vehicles (MAVs). The conversion of radio-frequency (rf) power into usable direct-current (dc) power is performed by a rectifying antenna, or rectenna. The emphasis of this thesis is the simulation and experimental study of various rectenna designs to determine which best provides high efficiency, stable output power, and lightweight design.

The analysis of rectenna design focuses on four subsystems: (1) the receiving antenna, (2) the matching sections, (3) the rectification, and (4) the post-rectification filter. Based on the findings of this research, the ultimate rectenna design implements a half-wave dipole antenna that performs full-wave rectification with two diodes. The post-rectification filter is implemented by a capacitor to obtain stable dc power. The final design achieved an efficiency of nearly 66% for input power in the range of 200 mW.

14. SUBJECT TERMS Rectenna, Wireless Power Transmission, Dipole Antenna, MAV		**15. NUMBER OF PAGES** 95
		16. PRICE CODE
17. SECURITY CLASSIFICATION OF REPORT Unclassified	**18. SECURITY CLASSIFICATION OF THIS PAGE** Unclassified	**19. SECURITY CLASSIFICATION OF ABSTRACT** Unclassified	**20. LIMITATION OF ABSTRACT** UU

THIS PAGE INTENTIONALLY LEFT BLANK

AN IMPROVED RECTENNA FOR WIRELESS POWER TRANSMISSION FOR UNMANNED AIR VEHICLES

Chun-Yi Liu
Captain, Republic of China Army
B.S., Chung Cheng Institute of Technology, 2005

Submitted in partial fulfillment of the
requirements for the degree of

**MASTER OF SCIENCE IN ELECTRONIC WARFARE
SYSTEMS ENGINEERING**

From the

**NAVAL POSTGRADUATE SCHOOL
September 2011**

Author: Chun-Yi Liu

Approved by: David C. Jenn
                    Thesis Advisor

                    Ric Romero
                    Second Reader

                    Dan C. Boger
                    Chair, Department of Information Science

THIS PAGE INTENTIONALLY LEFT BLANK

ABSTRACT

This thesis continues an NPS project related to wireless power transmission for micro air vehicles (MAVs). The conversion of radio-frequency (rf) power into usable direct-current (dc) power is performed by a rectifying antenna, or rectenna. The emphasis of this thesis is the simulation and experimental study of various rectenna designs to determine which best provides high efficiency, stable output power, and lightweight design.

The analysis of rectenna design focuses on four subsystems: (1) the receiving antenna, (2) the matching sections, (3) the rectification, and (4) the post-rectification filter. Based on the findings of this research, the ultimate rectenna design implements a half-wave dipole antenna that performs full-wave rectification with two diodes. The post-rectification filter is implemented by a capacitor to obtain stable dc power. The final design achieved an efficiency of nearly 66% for input power in the range of 200 mW.

THIS PAGE INTENTIONALLY LEFT BLANK

TABLE OF CONTENTS

THIS PAGE INTENTIONALLY LEFT BLANK

LIST OF FIGURES

x

THIS PAGE INTENTIONALLY LEFT BLANK

LIST OF TABLES

THIS PAGE INTENTIONALLY LEFT BLANK

LIST OF ACRONYMS AND ABBREVIATIONS

ADS	Advanced Design System
BPF	Bandpass Filter
CST	Computer Simulation Technology
CW	Continuous Wave
dc	Direct Current
DARPA	Defense Advanced Research Project Agency
FGCPW	Finite-width Ground Coplanar Waveguide
LPF	Lowpass Filter
LTSA	Linear Tapered Slot Antenna
MAV	Micro Air Vehicle
rf	Radio Frequency
SL	Slot Line
SPS	Solar Power Satellite
S-Parameters	Scattering Parameters
SSP	Space Solar Power
UAVs	Unmanned Air Vehicles
WPT	Wireless Power Transmission

THIS PAGE INTENTIONALLY LEFT BLANK

ACKNOWLEDGMENTS

I would like to express sincere thanks to my thesis advisor, Professor David C. Jenn, for his patience and encouragement throughout these nine months. He always put aside his precious time to discuss thesis topics with me and gave me strength to keep working on this project. I could not have completed this thesis without the assistance of Professor Jenn.

I would also like to thank Assistant Professor Ric Romero, who was my second reader for this thesis.

I am grateful to the Chung-Shan Institute of Science and Technology for providing this opportunity to study at the Naval Postgraduate School.

Finally, I would like to thank my family for their encouragement and understanding. Their support enabled me to graduate from the Naval Postgraduate School.

THIS PAGE INTENTIONALLY LEFT BLANK

I. INTRODUCTION

A. Background

The concept of wireless power transmission (WPT) dates back to the days of Heinrich Hertz and Nikola Tesla [1], who discovered that energy could be transported by electromagnetic waves in free space. Tesla considered the use of wireless power transmission employing low-frequency transmission, sustained by the earth's natural electromagnetic resonance. His concept is important to later studies of electromagnetic-wave propagation. There has been intense interest in WPT recently for a number of applications. These include remote propulsion of vehicles [2], transmission of solar power from space [3] and wireless battery charging [4]. A related area is energy harvesting, where stray electromagnetic fields from the many systems in the environment are collected and used as a free energy source [5].

Micro-air-vehicle (MAV) propulsion is the main application of interest in this research. MAVs are a category of unmanned air vehicles (UAVs) being developed around the world. The definition of an MAV, according to the Defense Advanced Research Project Agency (DARPA), is a fully functional UAV no larger than 15 cm in length, width, and height [6]. The main reason for using wireless power transmission for military ground-surveillance applications is to achieve unlimited duration of flight without requiring onboard fuel supplies. One application that employs a MAV remotely powered by a small ground station is illustrated in Figure 1.
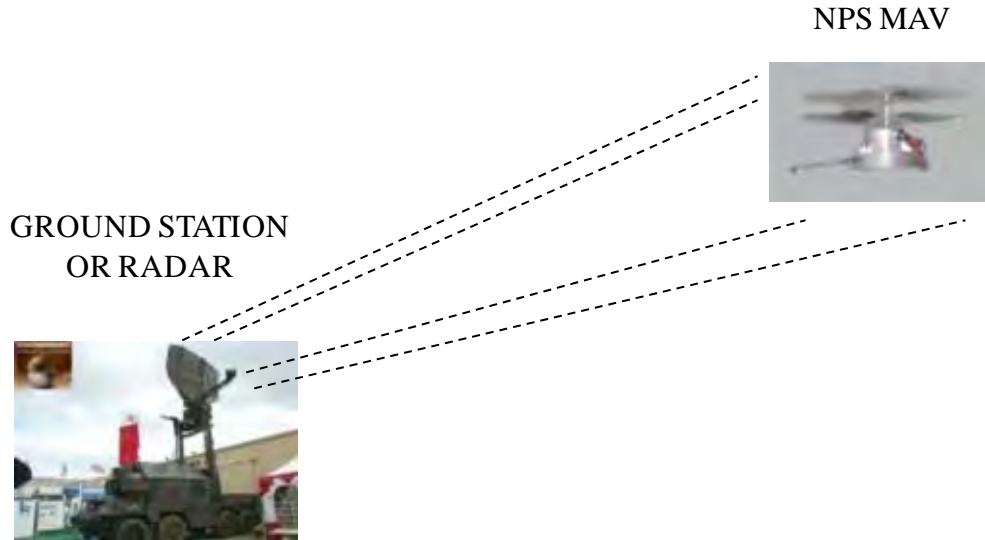
Figure 1.　　　Conceptual powering of an MAV by a ground station (From [6]).

In this thesis, a rectifying antenna (rectenna) system based on studies performed by Tan [6] and Toh [7] was re-evaluated, simulated, and refined. This study also looks at a new antenna design and a full-wave rectifier concept. In order to verify and validate the design of the rectenna model, many tradeoffs were made. Different rectenna designs were investigated, and an improved design was implemented in hardware.

The measured efficiency of the previous NPS rectenna was 26% to 37% [7]. This research changes the circuit design to yield better overall performance. The recommended design changes are shown to yield higher efficiency and lighter weight. The claimed theoretical efficiency of the rectifier designed by Toh [7] was approximately 26-37%, which was insufficient to power a micro air vehicle designed by Tsolis [8].

B.　OBJECTIVE

The purpose of this thesis is to verify and analyze the different designs of the rectenna system and make improvements. Since the primary application considered is UAV propulsion, an important requirement is to minimize the antenna and rectifier circuit's size and weight. A new dipole design is presented that is lightweight and compact. A full-wave rectifier circuit is proposed, which increases the output power over that of the half-wave rectifier design.

2

C.   THESIS OUTLINE

This thesis is divided into six chapters. The next five are organized as follows:

Chapter II introduces the development of WPT from the early 1950s through today. References to various WPT studies and applications are also covered in this chapter. An overview of related thesis projects that were conducted at the Naval Postgraduate School is presented.

Chapter III focuses on three different rectenna designs, the components of a rectenna circuit, and evaluation of various circuit designs by using Advanced Design System (ADS) 2009 software from Agilent Technologies. Analysis of the dipole antenna dimensions, Schottky diode, and substrate material are covered in this chapter. Chapter III also discusses the effects of pre- and post-rectification filtering. The design of a rectenna with and without filters is documented, and a comparative study of the performance of the pre-, post-, and no-filter designs analyzed.

Chapter IV discusses the impedance of the rectenna and dipole-antenna array.

Chapter V summarizes the findings of this research and presents conclusions and recommendations for future research.

THIS PAGE INTENTIONALLY LEFT BLANK

II. BACKGROUND

A. EARLY EXPERIMENTS WITH WPT

The concept of wireless power transmission (WPT) began in the 1900s. The objective of WPT is to transfer electrical power through space without the need for cables. Conventional communication systems such as radio and cell phones only transmit small amounts of energy, but WPT must transfer a significant amount of power in order to charge a battery or propel vehicles. A generic WPT block diagram is shown in Figure 2. A key component in the receiving system is the rectifying antenna, or rectenna.
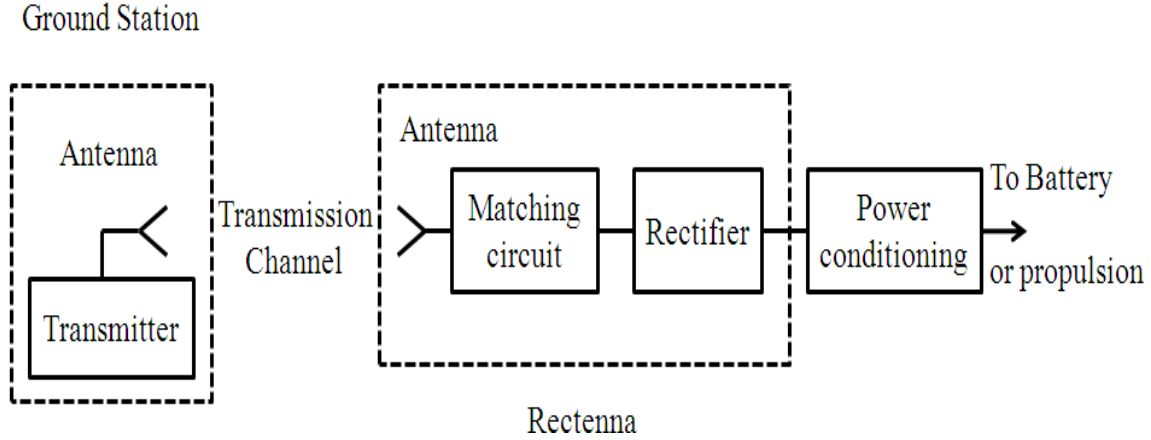
Figure 2.   Generic WPT-system block diagram.

Brown conducted wireless power-transmission research in 1963 [1]. In his article, Brown wrote a description of the development of WPT and the milestones along the way. Previously, Tesla carried out numerous experiments to transmit power without a wire at Colorado Springs in 1899 (Figure 3). A gigantic coil was built and fed with 300 kW of low-frequency power in order to produce very long and visible discharges from the sphere, but there is no record of whether any significant amount of power was collected at a distant location. Although Tesla's experiments ended due to lack of land and funding, his concept of efficient, wireless power transmission was important to future research.

5
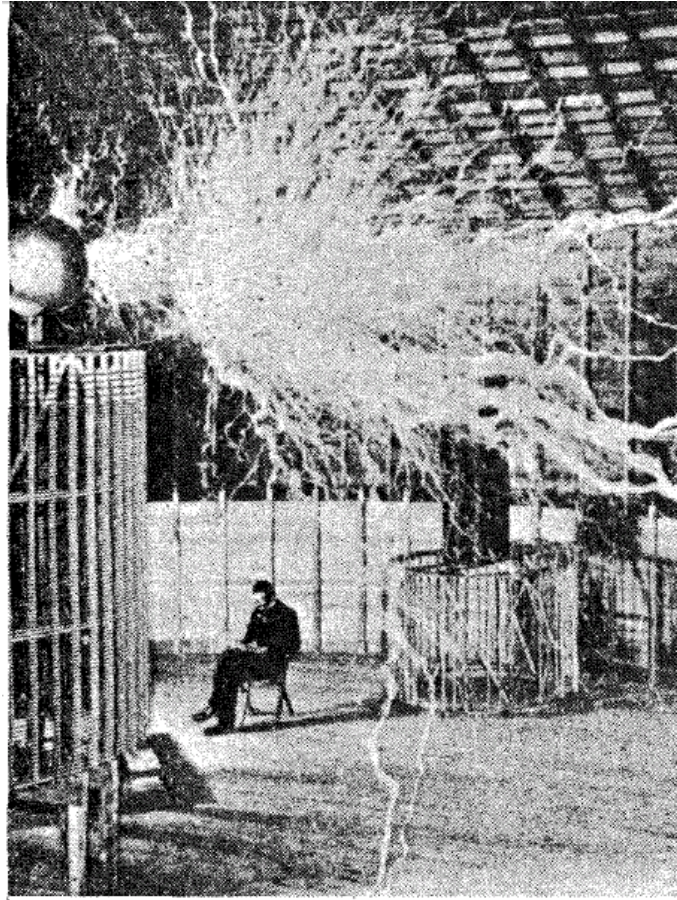
Figure 3.   Experiment with radio waves for power transmission (From [1]).

In the late 1930s, a further advance in WPT occurred with the invention of the klystron tube, which converted microwave power into dc power by using microwave power tube at one end and dc diode tubes at the other. Advances in the microwave-cavity magnetron led to higher efficiency for WPT applications during World War II.

In the 1950s, two advances were enabled by the invention of the amplifier tube, which created a larger amount of transmitting power [9] to drive an electromagnetic beam, and the focusing of electromagnetic power into a beam for high efficiencies [10]. In May 1963, Raytheon demonstrated the first microwave-power transmission system, which converted 400 W of CW power at the transmitter to 100 W of dc power to drive a motor.

In October 1964, a demonstration of microwave-powered helicopter flight up to 60 ft. above a transmitting antenna was presented (Figure 4). In November of that year, a nonstop, 10-hour hover was demonstrated.
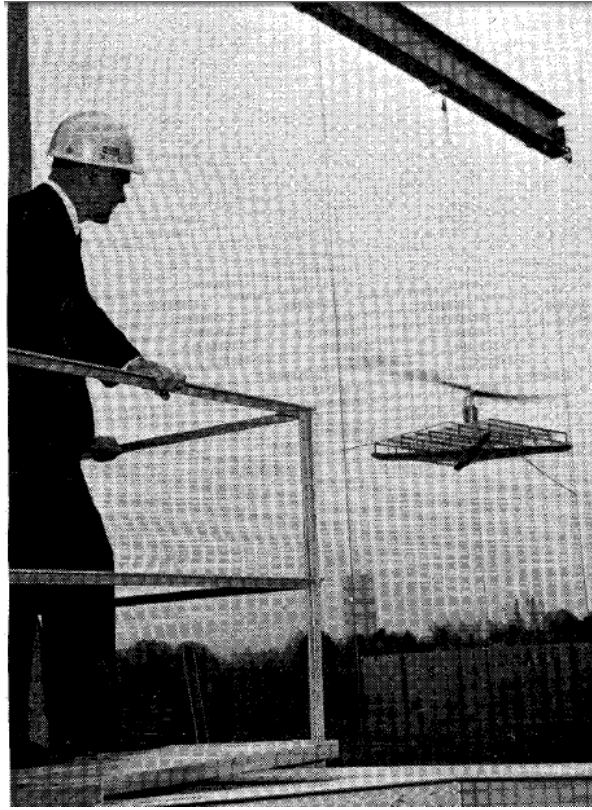
Figure 4.   A helicopter powered by WPT (From [1]).

The concept of a solar-power satellite (SPS) introduced in the 1960s also relied on WPT, as illustrated in Figure 5. In the SPS concept, solar energy collected in orbit is converted into microwave power for transmission to a large antenna on ground. With oil consumption increasing over the past years, WPT technology has become an alternative source of energy by transmitting collected solar power from satellites to an earth rectenna station. Solar energy transmitted by WPT is environmentally clean and available 24 hours a day from space by using satellites as collection stations. Although the SPS program ended in 1980, it redirected the design of the transmitter antenna to an active, phased array made from a large number of microwave generators instead of super power tubes.

For ground-based arrays, the low-cost, microwave-oven magnetron could be used directly in the SPS. Pacific Gas and Electric (PG&E) has recently funded a study to design a commercial SPS system [3].

Figure 5.   Satellite solar-power model (From [14]).

In the 1990s, the advancement of WPT related to the use of solid-state silicon-based PN junction diodes, which have a high turn-on voltage, and new GaAs Schottky diodes that have fast switching capability for the high-frequency rectification processes. Semiconductor devices were became suitable for achievement of high-rectification efficiency in WPT applications. The first fuel-less plane powered by microwave was produced by Joseph in September 1987 [2]. An array of antennas was used to transmit microwaves onto the plane disc with a dual-polarized rectenna. The airplane flew on beamed microwave for 20 minutes.

B.   RECENT DEVELOPMENTS IN WPT

Recently there has been increased activity in WPT. In a September 1999 article by Youn [11], a WPT system achieving a single rectenna conversion efficiency of 75.6% and an overall system efficiency of 33% are described.

Hagerty [12] proposed an array of 64 circularly polarized spiral elements and used a broadband-antenna array to convert more microwave power into dc power. The achievement of 20% efficiency over a frequency range of 2–18 GHz was reported.

A December 2002 survey article on space solar-power (SSP) program research was written by McSpadden [13]. McSpadden gave insight on achieving practical SSP and emphasized three critical components: the transmitter, beam control, and rectennas. Although it was acknowledged that the technology was immature, a strategic roadmap was highlighted for future investigation.

In [14], Goel proposed that a solar-power satellite could be placed in halo orbit to be fixed over the earth's midnight as the earth rotates. The proposed orbit, known as the trans-earth Lagrange point, obviates the need for a rotating joint between the solar array and microwave transmitter, making a simpler design possible.

C.   RECENT RESEARCH IN RECTENNAS

In [15], a dual-frequency. printed-diode rectenna system using a GaAs Schottky diode that could achieve 84.4% and 82.7% efficiency at 2.45 and 5.8 GHz, respectively, is reported. The dual-frequency rectenna system is illustrated in Figure 6.
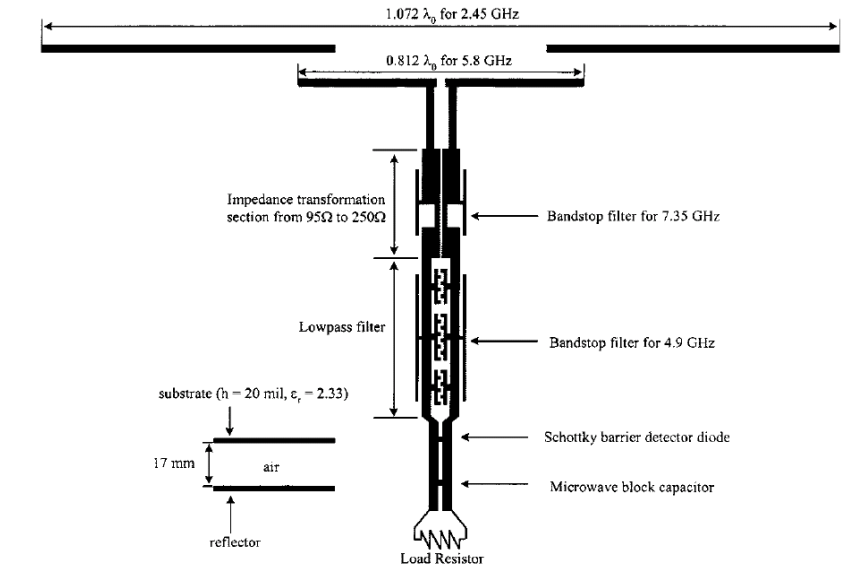
Figure 6.   Circuit configuration of the dual-frequency rectenna (From [15]).

Reference [16] by Strassner contains an article on a 5.8 GHz, circularly polarized rectenna design and array. Strassner demonstrated the feasibility of a rectenna array scaled 3 feet wide by 2 feet long and 4 inches tall, with an efficiency of 82% and output power of 7.6 W.

Reference [17] reports a circular-sector antenna using inset feeding in order to exhibit high reflection coefficients at the second and third harmonics generated by the diode. As illustrated in Figure 7, the rectenna can eliminate the need for a low-pass filter (LPF) placed between the antenna and the diode, as well as achieve a conversion efficiency of 77.8% at 2.4 GHz.
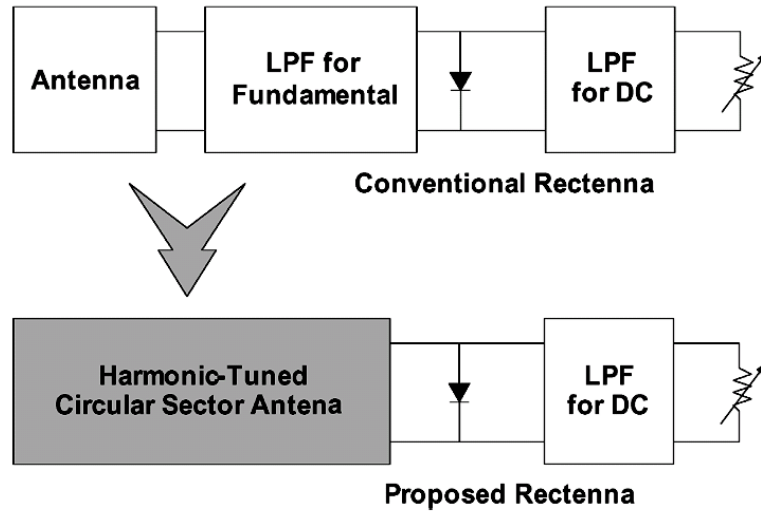
Figure 7.   Block diagram of the conventional and the proposed rectenna (From [17]).

In [18], Zbitou reported a monolithic rectifier design with a second diode acting as a variable resistor to achieve an overall efficiency of 65% at 2.54 GHz. He conducted the study using a GaAs, pseudomorphic, high-electron-mobility transistor process to develop a monolithic rectifier to minimize circuit dimensions. The dimension of the rectenna was 1340 μm by 476 μm.

The use of full-wave rectification for rf-to-dc conversion showed that 70.69% rectenna efficiency could be achieved with an input power of 45 mW [19]. The conversion efficiency depends on load resistance, due to the internal resistance of the rectenna system (Figure 8).
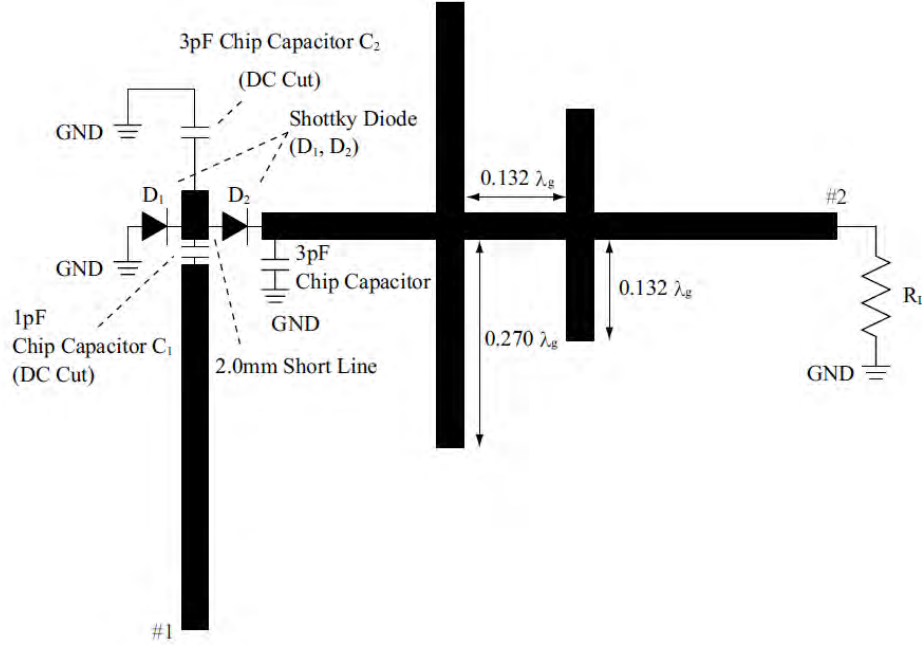
Figure 8.   Full-wave rectification (From [19]).

A recent article by Olgun [20] reported that a rectenna system combining a two-stage, zero-bias Schottky diode with a miniature antenna could achieve 70% efficiency at 2.4 GHz. The diodes are in parallel to rf signals, but appear in series for the dc circuit in order to produce doubled voltage. The circuit layout of the rectenna is depicted in Figure 9.
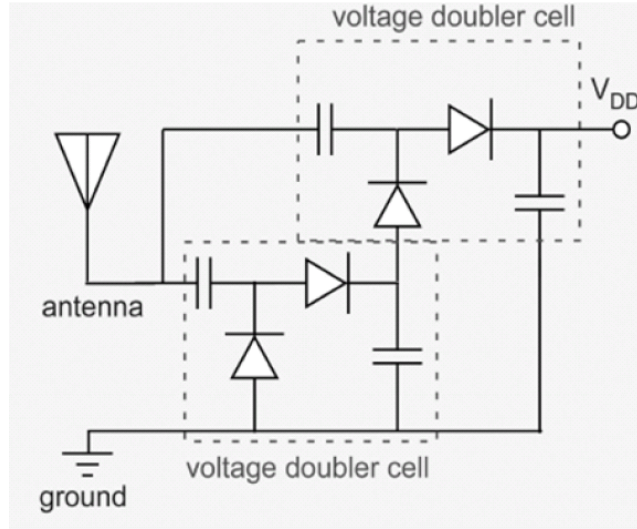
Figure 9.   Circuit design of the rectenna (From [20]).

D.   PREVIOUS NPS RESEARCH

Students at Naval Postgraduate School have looked into aspects of WPT for MAV propulsion. Vitale [21] utilized a metal semiconductor diode to design a rectification circuit and was able to experimentally determine the scattering parameters (S parameters) of the diode. He highlighted that future research into employing GaAs Schottky diodes for higher rectification efficiency and using a high power source for examining improvement on the MAV antenna design.

Tsolis [8] extended Vitale's work by using Schottky diodes with a patch antenna, but efficiency was verified to be only 7%, due to the mismatch of impedance. Tan [6] investigated various designs of antennas and concluded that a round-patch antenna and sixth-order filters were the better design. He recommended that further analysis into building rectenna to determine the fabrication robustness and conversion efficiency.

Toh [7] improved Tan's design by matching the impedance of the rectenna system. Toh introduced an impedance-matching unit and simulated his design using software. The prototype of the rectenna system was fabricated and tested. The overall efficiency of a single rectenna element varied between 26% and 37%.

E.   SUMMARY

In this chapter, the major milestones in the development of WPT were highlighted and a brief history of WPT was covered. Much research has been conducted to determine the feasibility of implementing WPT and its applications, which range from miniaturized versions of remotely powered vehicles to large-scale systems. In the next chapter, rectenna design is addressed in detail.

THIS PAGE INTENTIONALLY LEFT BLANK

III. RECTENNA DESIGN

A. DISCUSSION OF RECTENNA DESIGN

1. General Rectenna Design

A rectifying antenna (rectenna) receives a microwave signal at the antenna and converts it to direct current. It should do this as efficiently as possible and provide a clean, constant, low-ripple voltage. Typically, a rectenna is composed of four components: (1) an antenna, (2) a pre-rectification filter, (3) a rectification diode, and (4) a post-rectification filter [7]. The basic configuration of the previous NPS rectenna systems is depicted in Figure 10.
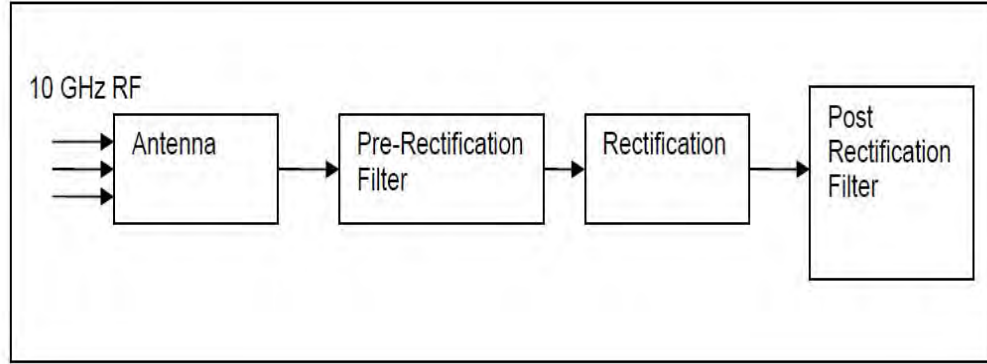
Figure 10. Basic configuration of NPS rectenna system (From [7]).

There are many candidate antenna designs, such as half-wave dipole, horn, parabolic antenna, and microstrip antenna. Some of these can be discarded for this application, due to their weight or size. In reference [8], Tsolis concluded that a circular-patch antenna was preferred, in part due to its capability of reducing the reradiation of harmonics. Figure 11 shows the S_{11} (return loss) response of a circular-patch antenna. Ideally, the return loss of a circular-patch antenna is about 50 dB. In practice, the return loss is likely to be 15 dB to 20 dB. (Return loss is a positive quantity equal to the negative of S_{11} in dB.)

15
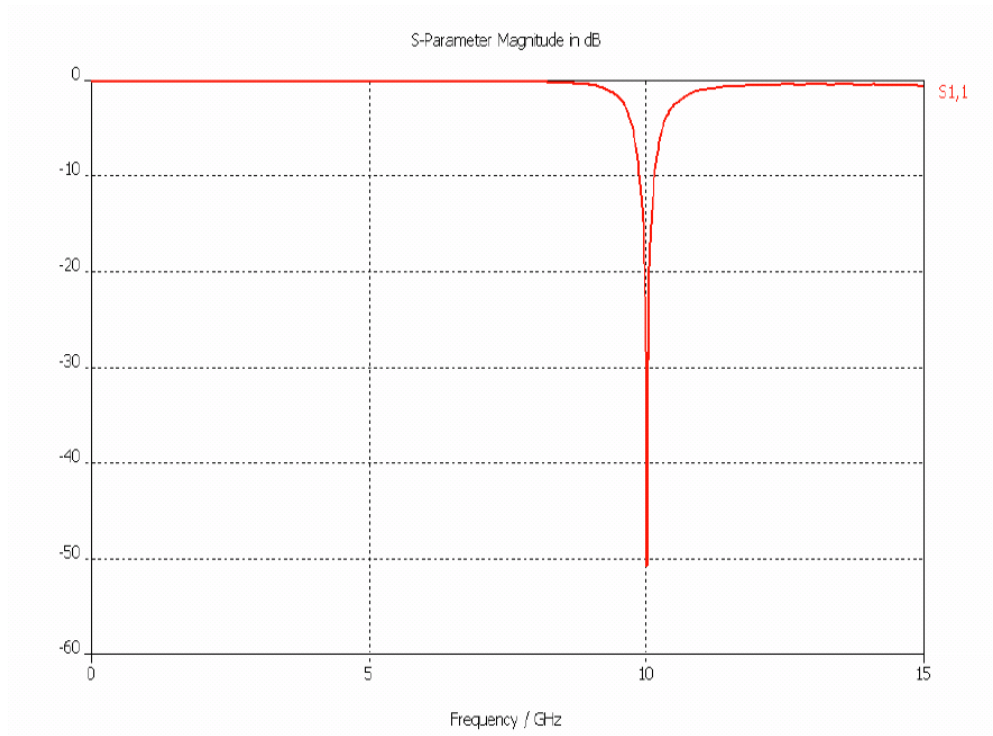
Figure 11. S_{11} frequency response of circular-patch antenna design (From [7]).

The antenna feeds directly into a pre-rectification filter. It allows the 10 GHz operating frequency to pass and prevents interference signals and re-radiation of higher-order harmonics generated by the diode. It also helps provide a constant load impedance for the antenna. Tan [6] selected a sixth-order LPF instead of a fourth-order LPF, due to its better response at 10 GHz. Figure 12 shows that the S_{12} (insertion loss) is 0.078 dB (insertion loss is the negative of S_{12} in dB.)
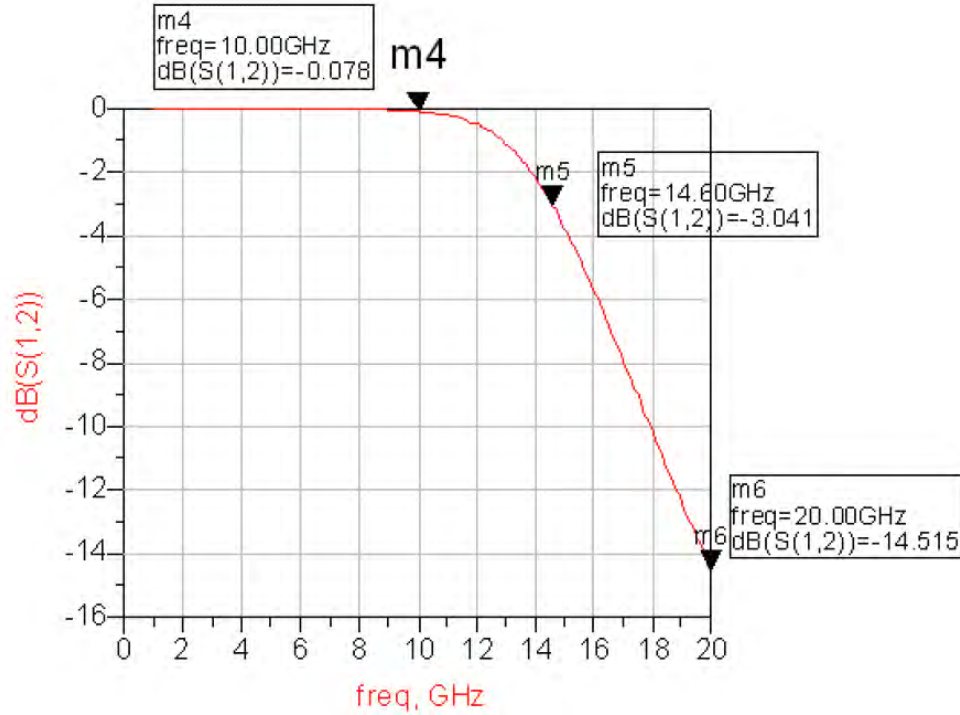
Figure 12.　　Simulated response of sixth-order low pass filter using ADS software (From [7]).

Rectification is the key function of the rectenna: converting microwave rf energy into dc power. In reference [8], the Schottky diode was used as the rectifying device, due to a high switching capacity that enables it to follow a high-frequency input signal. A commercial Avago HSMS8101 was used in the NPS rectenna system [7], [8]. The S_{21} response of the Schottky diode is depicted in Figure 13. The value of S_{21} is about -0.5 dB at 10 GHz [7].
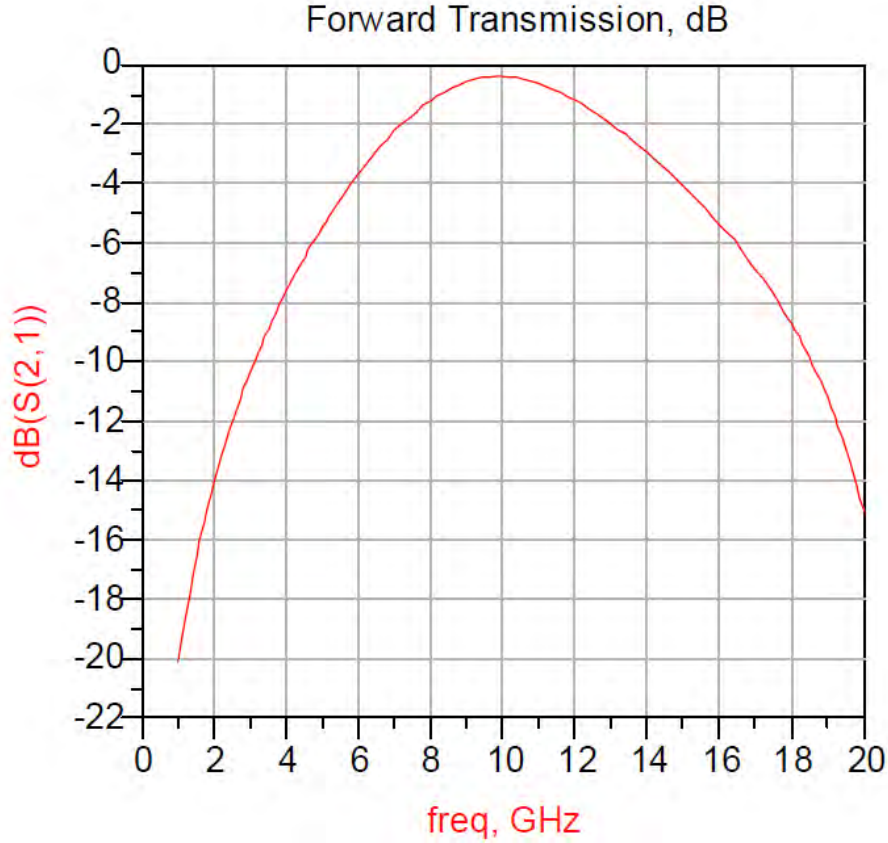
Figure 13.   Simulated response of Schottky diode using ADS software (From [7]).

A post-rectification filter is used to extract the dc component and produce a smooth transient for output dc power. Toh [7] developed a post-rectification filter by simply using a 47 pF capacitor in the circuit design.

Tsolis [8] studied the MAV motor prototype DMMK06-10 and measured data for the motor. Toh [7] confirmed the characteristics of the motor given in Table 1. In order to hover the weight of 10 g with 0.952 W, Toh concluded that at least 22 rectenna elements are needed, with each rectenna producing a maximum power of 75 mW. He also implemented a half-wave rectenna and measured the maximum power produced by a single rectenna to be 41.15 mW. In order to hover the MAV, the present research needed to produce more dc power from each rectenna than the previous half-wave rectenna and design a lighter-weight rectenna circuit.

18

DMMK06-10 Motor's characteristics							
Weight (g)	net	5	10	15	20	25	30
Voltage (V)	5.5	7	8.1	9.9	11.5	14	16
Current (A)	0.1	0.136	0.17	0.22	0.264	0.319	0.357
Resistance (Ω)	54.9	51.4	47.4	45	43.5	43.8	44.8
Power (W)	0.55	0.952	1.3817	2.1780	3.0360	4.4660	5.7120
Round Per Minute	1200	1440	1620	1740	1770	1800	2100

Table 1.   Measured data for the MAV motor (From [7]).

2.   Antenna Design

In order to obtain a lightweight rectenna design for MAV applications, we discuss possible changes or removal of components of the rectenna. First, we propose using a half-wave dipole antenna instead the original circular-patch antenna to reduce weight. Figure 14 illustrates the structure of the half-wave dipole antenna over a ground plane modeled in CST Microwave Studio. The dipole has a unique design: only one arm is fed by the microstrip line, while the other arm is open. As will be discussed in a later section, this represents the situation that occurs when the dipole is used in a full-wave rectenna.

19
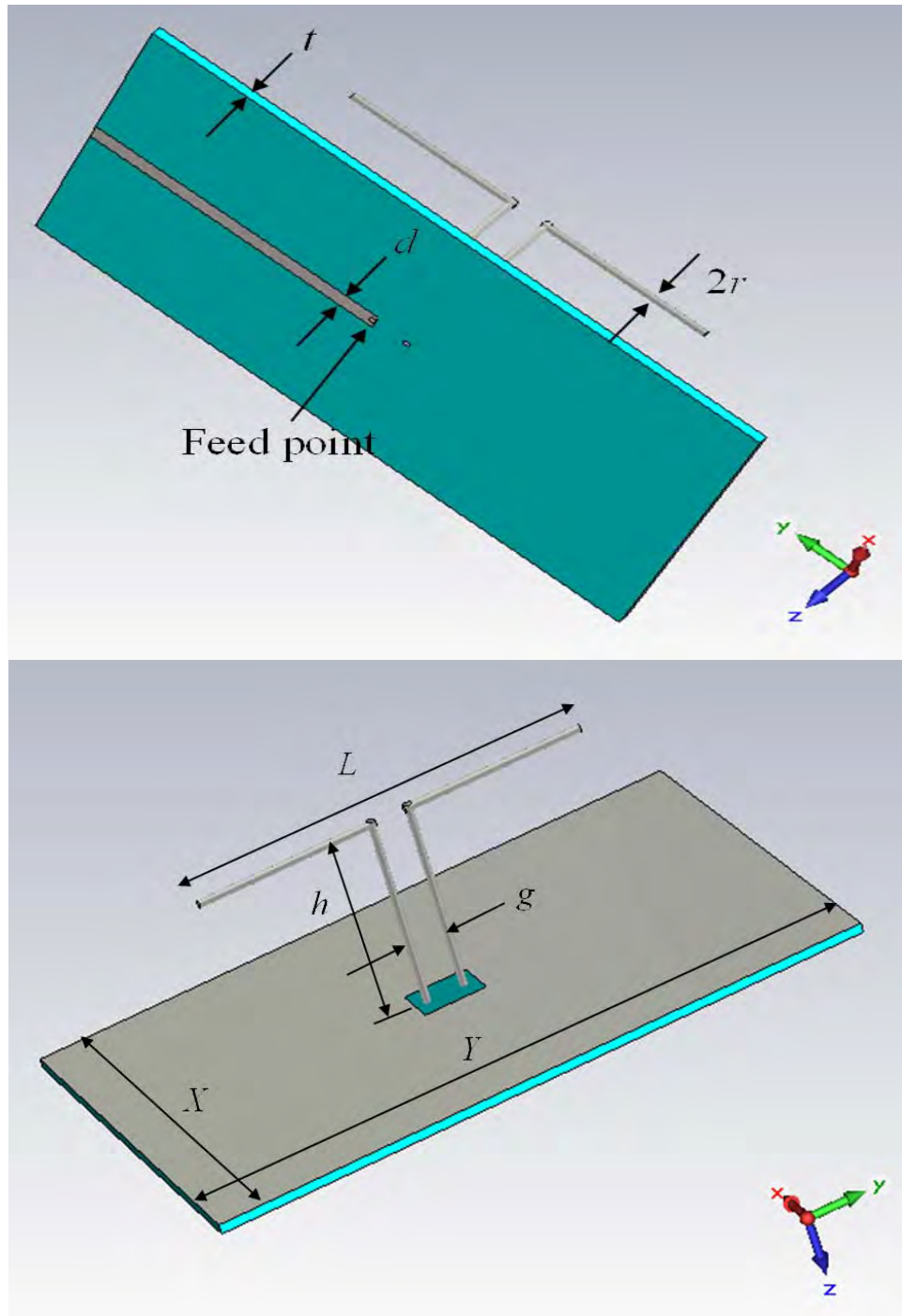
Figure 14.   Two views of the half-wave, dipole-antenna structure.

Table 2 lists the design specifications for the data in Figure 15 through 17.

Half-wave dipole's specifications			
Dipole wire radius (r)	0.25	Gap width (g)	1.5
Substrate height (t)	0.508	Dipole height above ground (h)	9
50 ohm line width (d)	1.6829	Sample width (X)	25
Dipole length (L)	25	Sample length (Y)	35

Table 2.   Design specifications for the half-wave dipole antenna.

Figure 15 shows the S_{11} response of the half-wave dipole antenna. The return loss is about 23.5 dB at 10 GHz. The impedance of the antenna is 44+j1.6 Ω at 10 GHz as noted on the Smith chart in Figure 16.
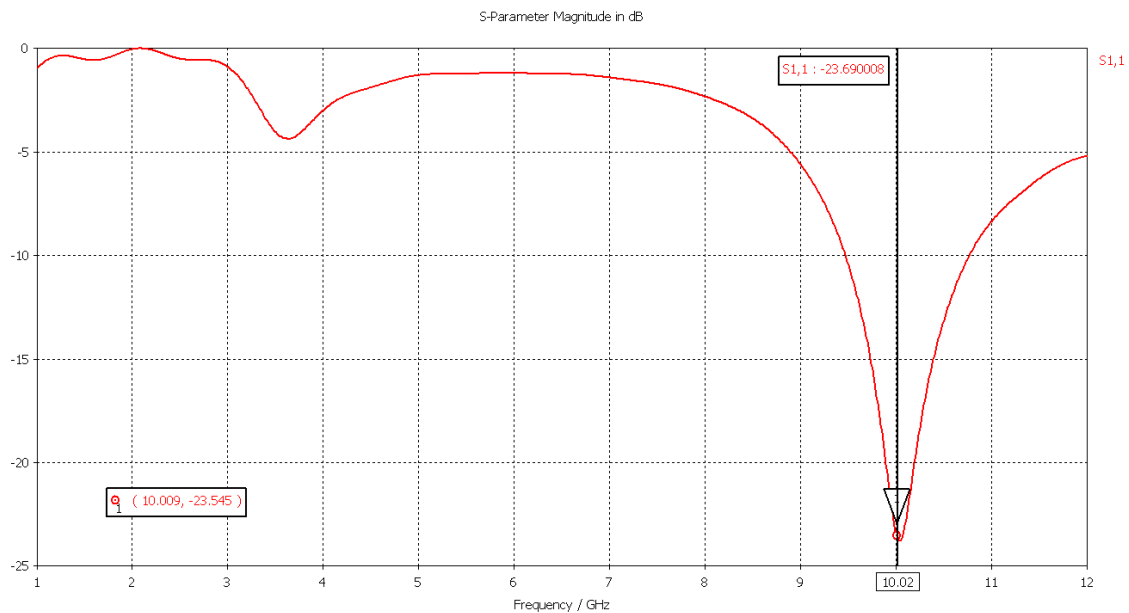
Figure 15. S_{11} frequency response of half-wave, dipole-antenna design.

21
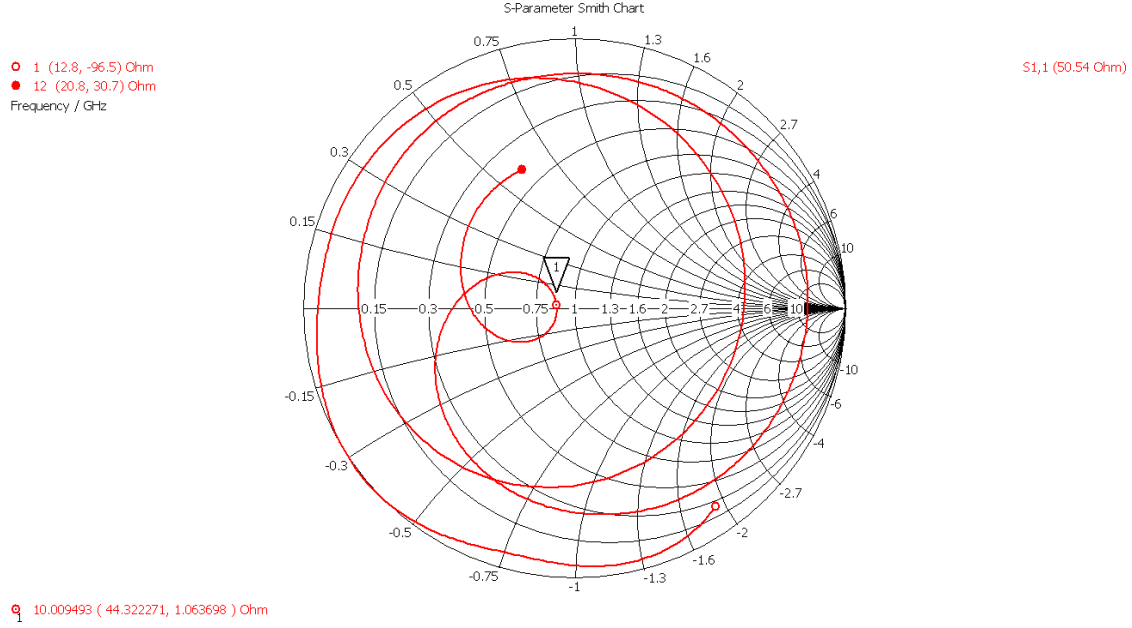
Figure 16.   Smith chart of the half-wave, dipole-antenna design**.**

The pattern, gain, and radiation efficiency of the antenna are given in Figure 17. The coordinate system is defined in Figure 14. The pattern plotted is $|E| = \sqrt{|E_\theta|^2 + |E_\phi|^2}$. The pattern gives good coverage over a wide range of angles. The large backlobe is from radiation by the microstrip feed line. It will be shielded in the final design. The return loss and pattern were found to be sensitive to the ground-plane size and dipole height. Smaller ground planes required a higher dipole for a good impedance match. From the simulation, we observe that using a half-wave dipole antenna has acceptable return loss and pattern.

Type	Farfield
Approximation	enabled (kR >> 1)
Monitor	farfield (f=10) [1]
Component	Abs
Output	Directivity
Frequency	10
Rad. effic.	0.01477 dB
Tot. effic.	-0.005285 dB
Dir.	6.161 dBi
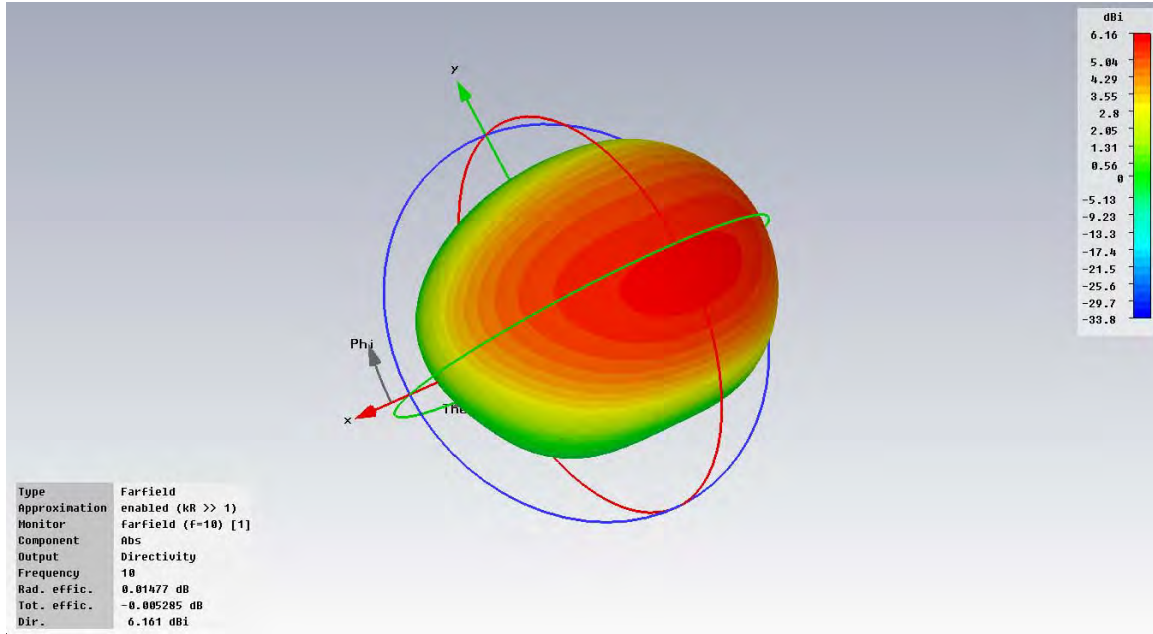
Figure 17.   Three-dimensional, far-field radiation pattern of the half-wave, dipole-antenna design**.**

3.   Power Budget

In this section, we introduce the effective area of the transmitting and receiving antennas and calculate the power density in order to obtain the required transmitter power for various distances. Figure 18 shows the geometry.
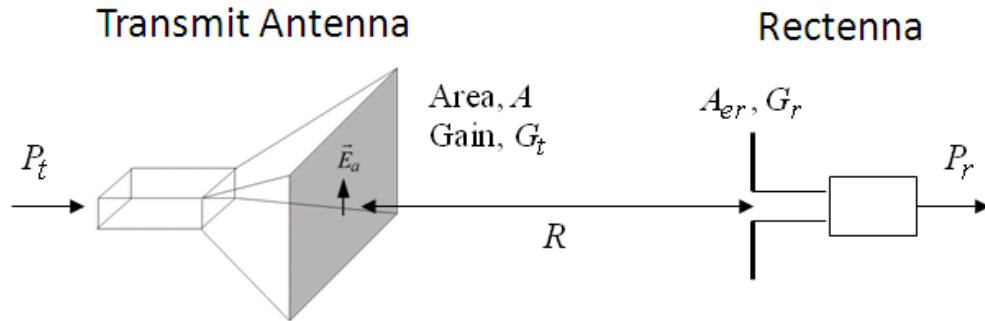
Figure 18.   Diagram of the transmit antenna and rectenna**.**

The effective area of the dipole antenna over a perfect ground plane is calculated using:

$$A_{er} = \frac{G_r \lambda^2}{4\pi} \tag{3.1}$$

where G_r is the gain of the dipole antenna and λ is the wavelength at 10 GHz. From Figure 17, the gain is 6.16 dB = 4.13. Using Eq. (3.1), the effective area of the dipole antenna is 2.96×10^{-4} m^2. The power density W_i transmitted by the horn antenna at distance R can be expressed as

$$W_i = \frac{P_t G_t}{4\pi R^2} = \frac{4\pi P_t \frac{A_{et}}{\lambda^2}}{4\pi R^2} = \frac{P_t A_{et}}{\lambda^2 R^2} \tag{3.2}$$

where P_t is the transmitted power, A_{et} is the effective area of the horn antenna, and R is the distance between transmitting and receiving antennas. The effective area of the horn antenna is the physical area (A) times the efficiency, e_t. Assuming horn dimensions of 3 inches by 4 inches and an efficiency of 0.7, $A_{et} = 0.0054$ m^2, the power P_r received by dipole antenna can be expressed as

$$P_r = W_i A_{er} = \frac{P_t A_{et} A_{er}}{R^2 \lambda^2}. \tag{3.3}$$

Using Equation (3.3), the required transmitting power versus the distance between transmitting and receiving antennas to obtain 200 mW of received power is given in Figure 19. From Figure 19, the transmitted power is 1.35 W for the distance of 30 cm, and the received power will be 200 mW. This analysis assumes the distance R is in the far field of the horn antenna.
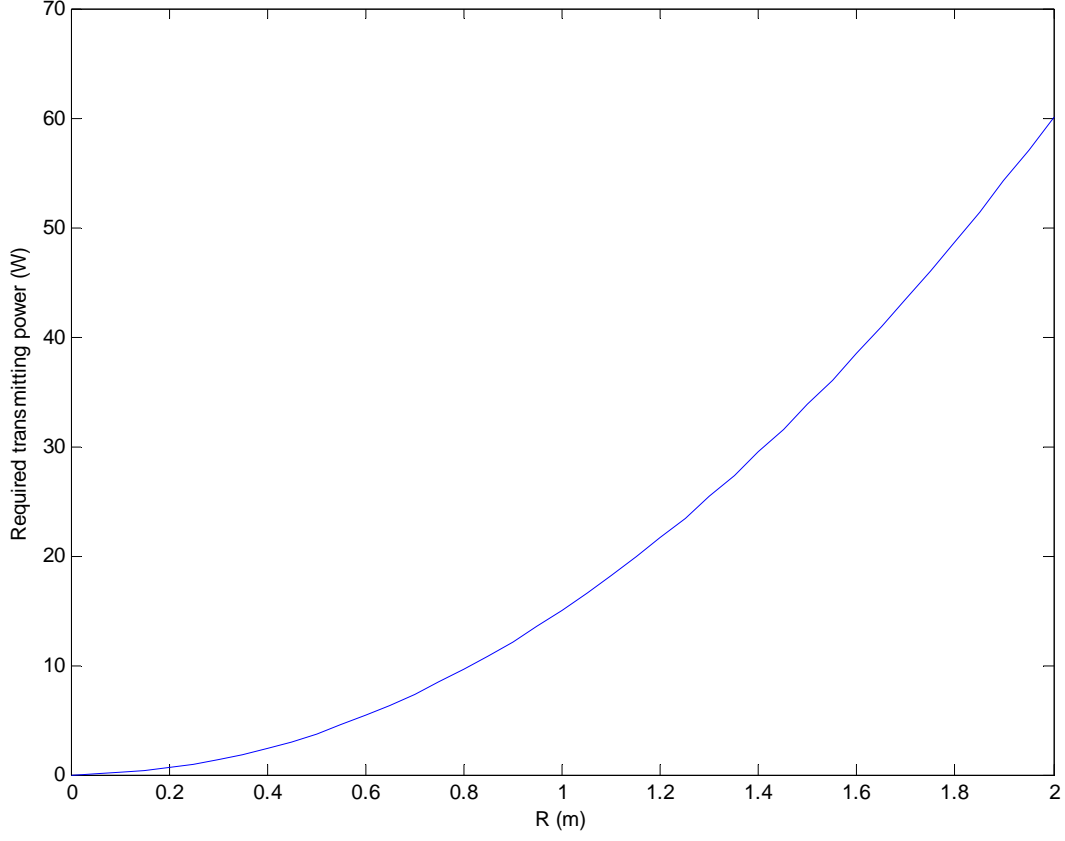
Figure 19.   Required transmitting power versus distance with 200 mW
received power.

Next, we evaluate the various rectenna configurations by simulating the
conversion efficiency and discuss the effect of changing the position of the pre-
rectification filter in rectenna design by analyzing the harmonics in the frequency domain.

B.   COMPARISON OF DIFFERENT DESIGNS USING ADS

In this section, we simulate the rf-to-dc efficiency of different rectenna designs,
such as a half-wave-rectification rectenna, hybrid rectenna, and full-wave rectenna.
Agilent ADS2009 is used to evaluate and compare the performance of the various
designs. This software provides numerous simulation technologies, covering issues such
as electromagnetic-field simulation and frequency and time-domain circuit simulation. To
compare performance with the NPS rectenna design, we model the original rectenna
circuit of Toh [7] using the HSMS8101 Schottky diode and sixth-order LPF.

1. Half-Wave-Rectification Rectenna Design

The half-wave-rectification rectenna has the advantage of simple circuit layout and ease of fabrication as a microstrip structure [22]. A block diagram of a half-wave-rectification rectenna is depicted in Figure 20.
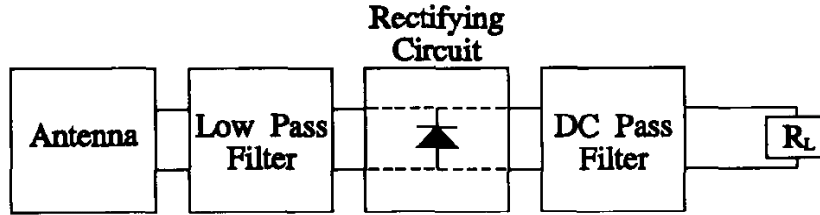
Figure 20.   Block diagram of half-wave rectification rectenna (From [22]).

In references [6], [7] a half-wave rectifier design was used. The circuit layout of the rectenna is given in Figure 21.
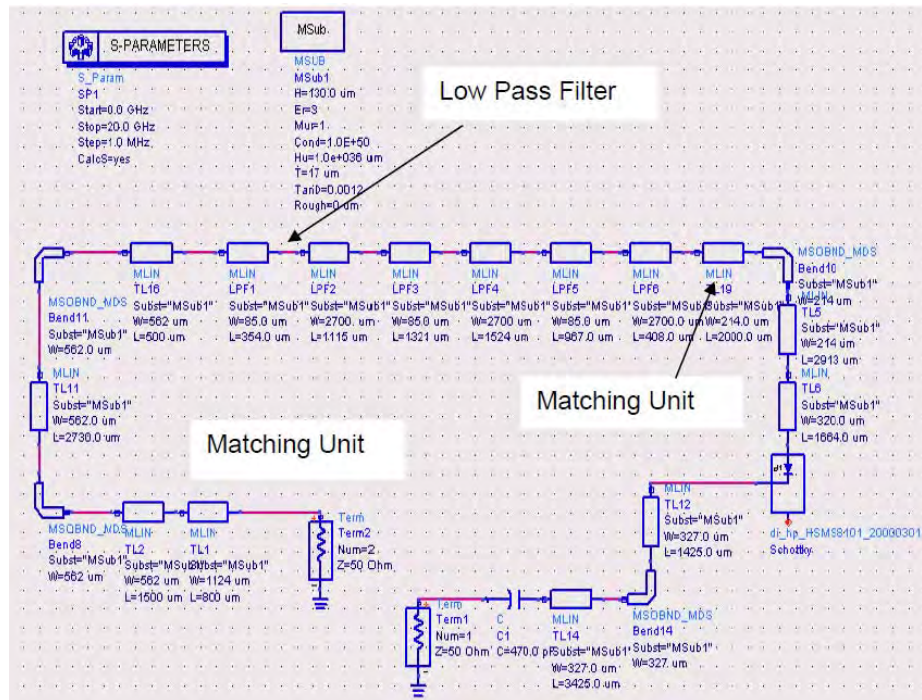
Figure 21.   ADS S-parameter circuit model of Toh's rectenna (From [7]).

Toh removed the dc pass filter because it was too small to solder correctly and it was found not to significantly affect output [7]. Omitting this component results in some ripple in the output dc; however, to minimize size and weight, the low-pass filter is possibly a component that can be omitted for some circuit designs. Figures 22 to 24 illustrate three different circuit designs of a half-wave rectenna that will be simulated in ADS. The three half-wave rectifier designs are: (1) with a pre-LPF, (2) with a post-LPF, and (3) without any LPF.
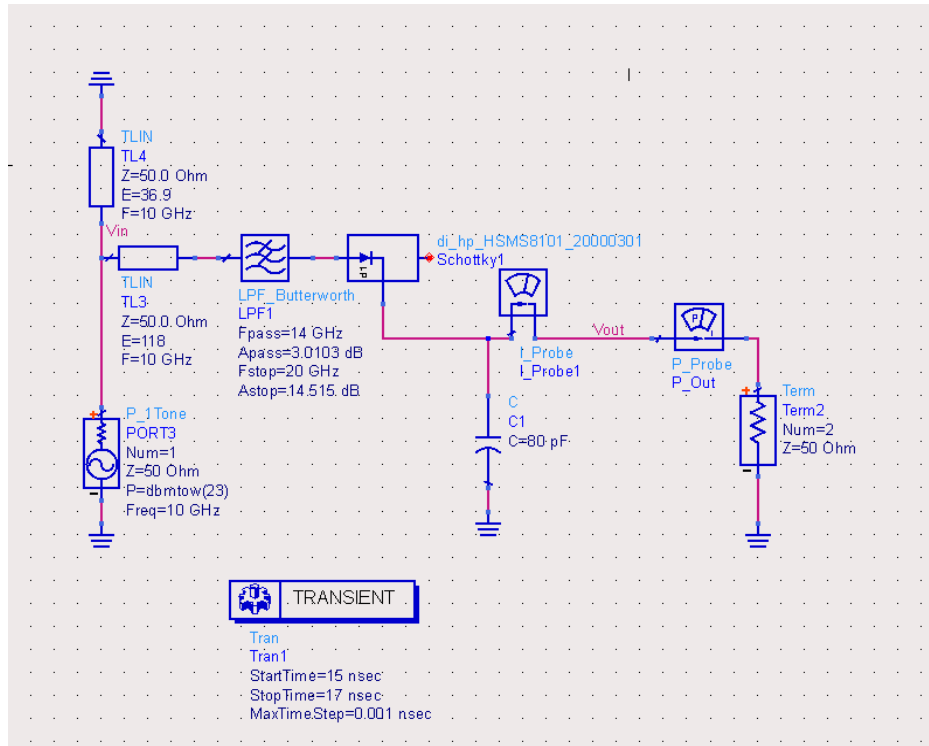
Figure 22.   ADS model of a half-wave rectenna design with a pre-LPF**.
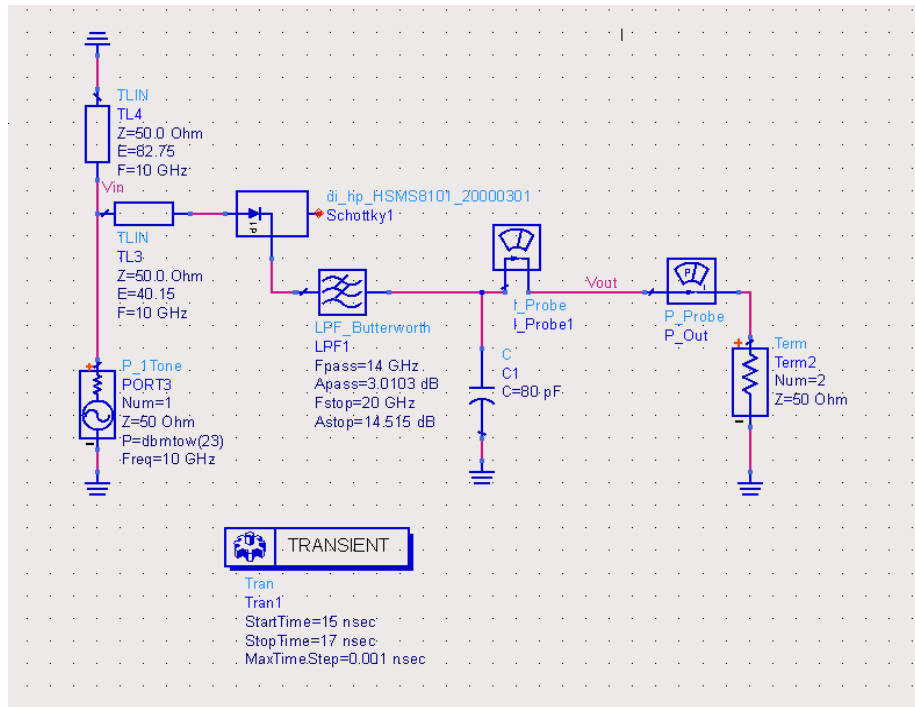
Figure 23.   ADS model of a half-wave rectenna design with a post-LPF.
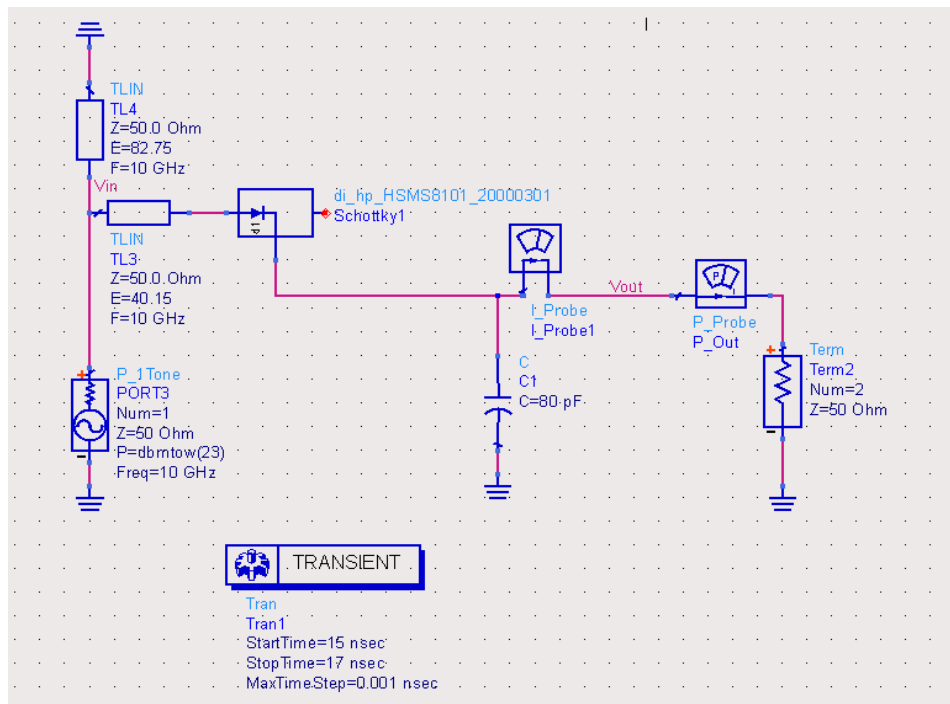
Figure 24.   ADS model of a half-wave rectenna design without LPF.

28

All three designs utilize a capacitor after the diode. In reference [21], Vitale noted that the output voltage when the diode is not conducting is compensated for by the discharge of the filter capacitor. It can be expressed as

$$V_{out}(t) = V_P e^{-t/R_L C} \tag{3.4}$$

where V_P is the peak voltage of the rectified signal, R_L is the load resistance, and C is the filter capacitance. For $R_L C \gg T$, the exponential can be approximated by $\left(1 - T/R_L C\right)$ and the minimum output voltage can be expressed as

$$V_{min} = V_P \left(1 - \frac{T}{R_L C}\right) \tag{3.5}$$

where T is a full period of the input sinusoid. He also determined that the output dc voltage V_{out} is approximated by the average voltage between the peak voltage and the minimum output voltage

$$V_{out} = V_P \left(1 - \frac{1}{2fR_L C}\right). \tag{3.6}$$

Figures 25 to 27 illustrate the output dc power produced by the three different circuit designs of a half-wave rectenna that were simulated in ADS.
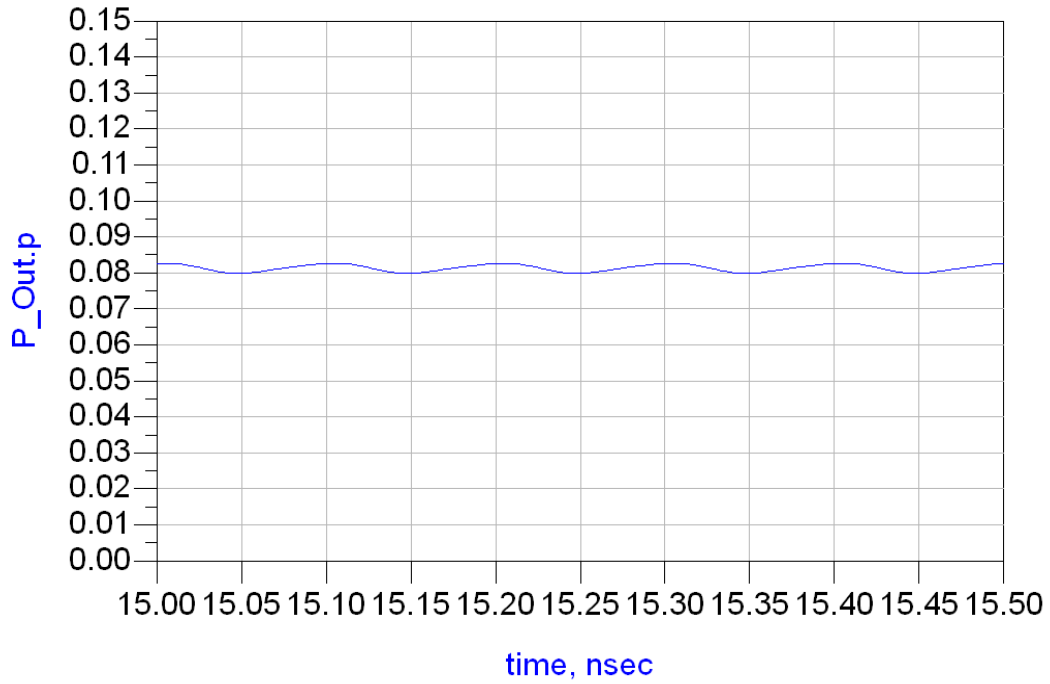
Figure 25.   Output power (watts) versus time for a half-wave rectenna design with a pre-LPF.
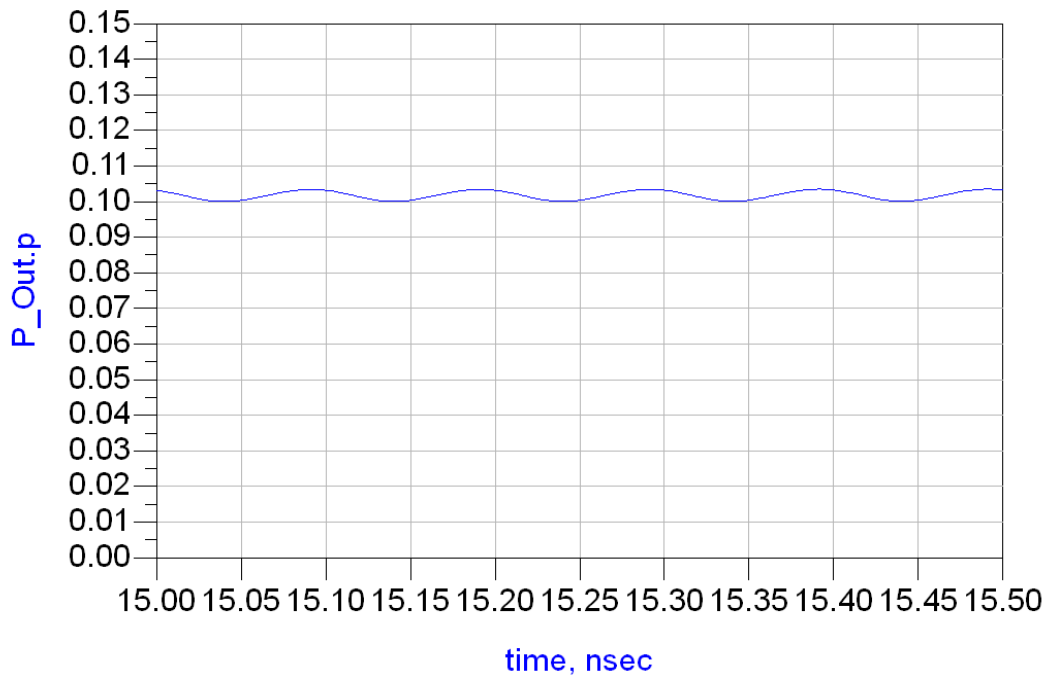
Figure 26.   Output power (watts) versus time for a half-wave rectenna design with a post-LPF.

30
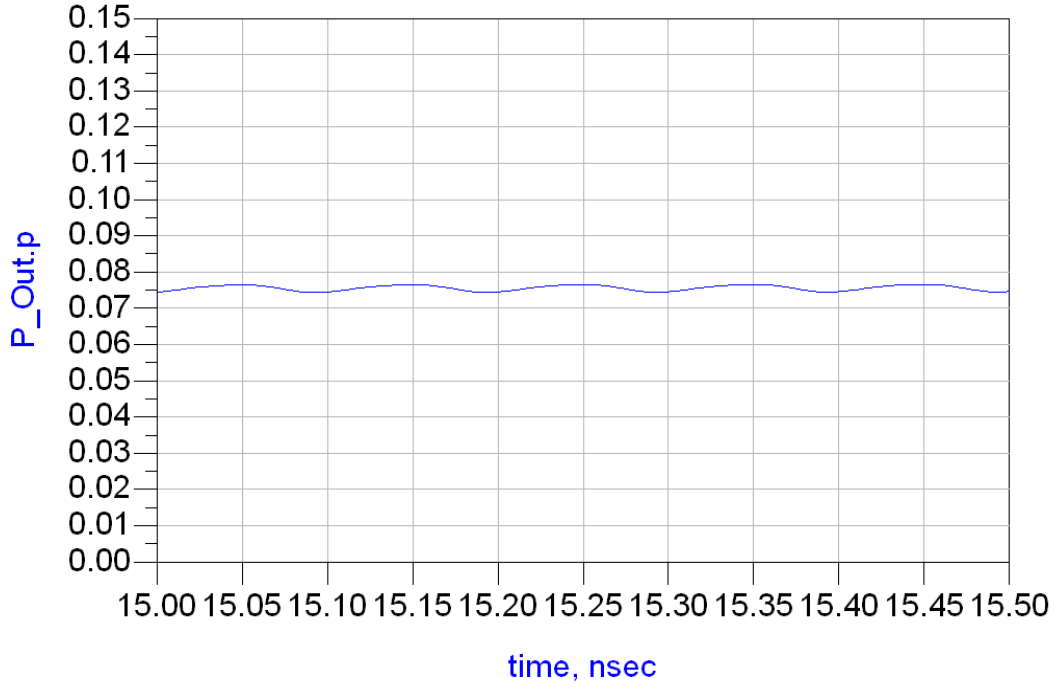
Figure 27.   Output power (watts) versus time for a half-wave rectenna design without LPF.

In addition, rf-to-dc conversion efficiency η in percent is calculated as follows:

$$\eta = \frac{\left(V_{DC}/R_L\right)}{P_{RF}} \times 100 \qquad (3.7)$$

where V_{DC} is dc output voltage, R_L is load resistance, and P_{RF} is microwave input power.

The simulated conversion efficiency of the half-wave rectennas is compared by using Equation (3.7). In Figure 28, the efficiency of the rectenna with post-LPF is higher than those for the pre-LPF and no LPF at their highest power levels. In comparison to the other designs shown in Figure 28, the design with post-LPF is able to convert wireless power to dc power with an efficiency of 54.3% at an input power of 150 mW, but the design with pre-LPF only achieves an efficiency of 45.8% at the same input power. In specific applications with input power smaller than 100 mW, we prefer the half-wave-rectification rectenna with pre-LPF to achieve a high conversion efficiency.

31
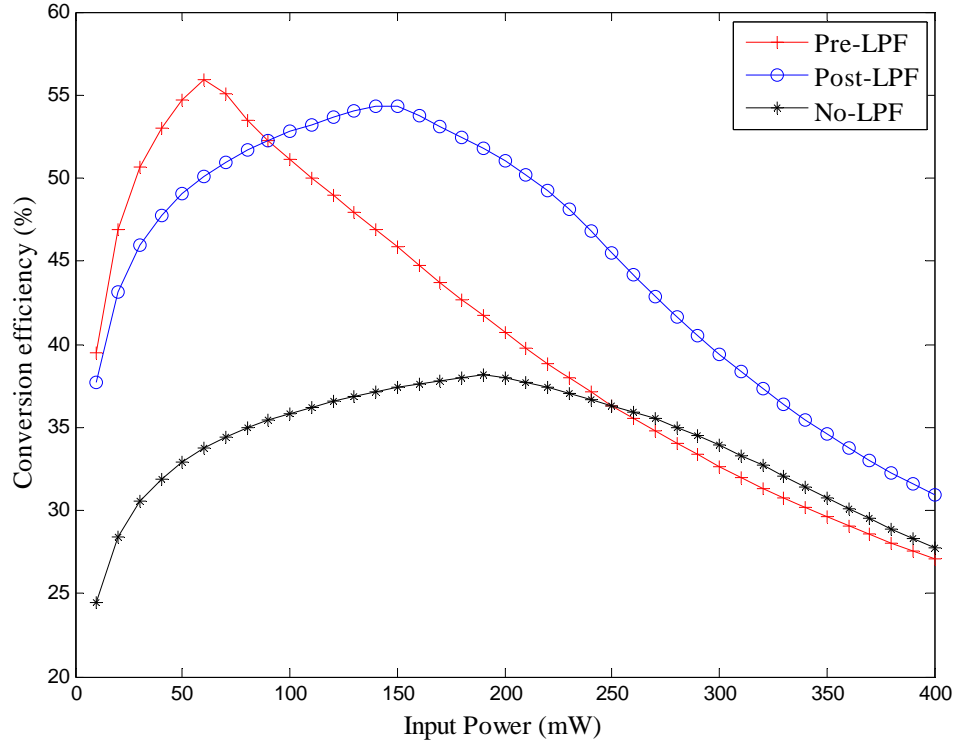
Figure 28.   Conversion efficiency of simulated half-wave rectenna designs using ADS.

2.   Hybrid Rectenna Design

In reference [18], Zbitou developed hybrid rectenna that achieved a conversion efficiency of 56% at 2.45 GHz. The block diagram of the hybrid rectenna is depicted in Figure 29. The function of the second diode is to provide a variable resistance in series with the load.
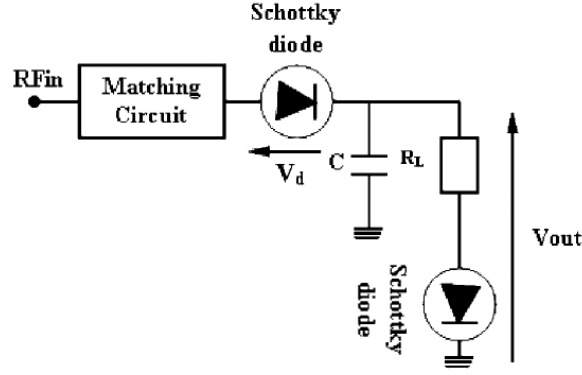
Figure 29.   Block diagram of hybrid rectenna (From [18]).

Zbitou considered the dc equivalent circuit of the Schottky diode as a voltage source in series with the junction resistance R_j and that the output voltage of the rectifier can expressed as

$$V_{out} = V_{DC} \frac{R_L}{R_L + R_j} \tag{3.8}$$

where V_{DC} is the dc part of the diode junction voltage and R_j is the junction resistance of the Schottky diode. R_j is obtained by differentiating the diode voltage-current characteristics and is given by [18]

$$R_j = \frac{nKT}{q(I_s + I_b)} \tag{3.9}$$

where n is the diode ideality factor, K is Boltzmann's constant, q is the electronic charge, I_s is the diode saturation current, I_b is the external bias current, and T is the temperature of the diode in degrees Kelvin. For the HSMS2820 diode, R_j is approximately 1.7 MΩ at ambient temperature, which tends to decrease the value of V_{out}, as evident from Equation (3.8). According to Equation (3.8), an increase in voltage at low power levels can be obtained when a variable resistance, which fluctuates as R_j, is connected in series with R_L. The value of this variable resistor must change with the

rectified current. Thus, Zbitou employed a technique using the same Schottky diode in series with R_L, in the dc portion of the rectifier, to act as a variable resistor (due to its current dependence in the junction resistance).

Three variations of the hybrid circuit are evaluated. Two incorporate an LPF (Figures 30 and 31). The third eliminates the LPF in order to minimize size and weight (Figure 32).

Figure 30.   ADS model of a hybrid rectenna design with a pre-LPF.
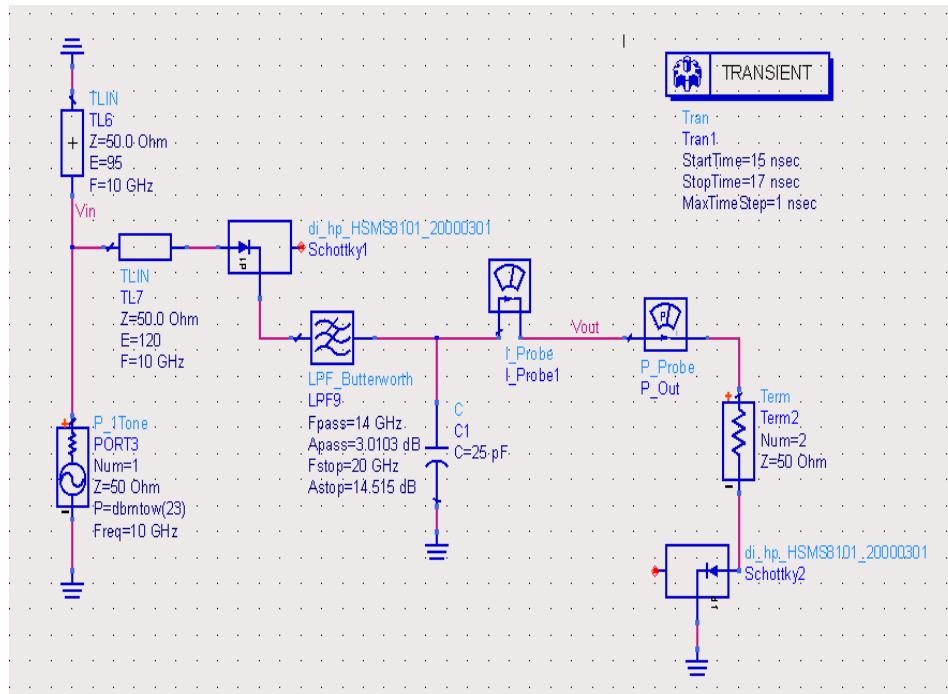
Figure 31.   ADS model of a hybrid rectenna design with a post-LPF.
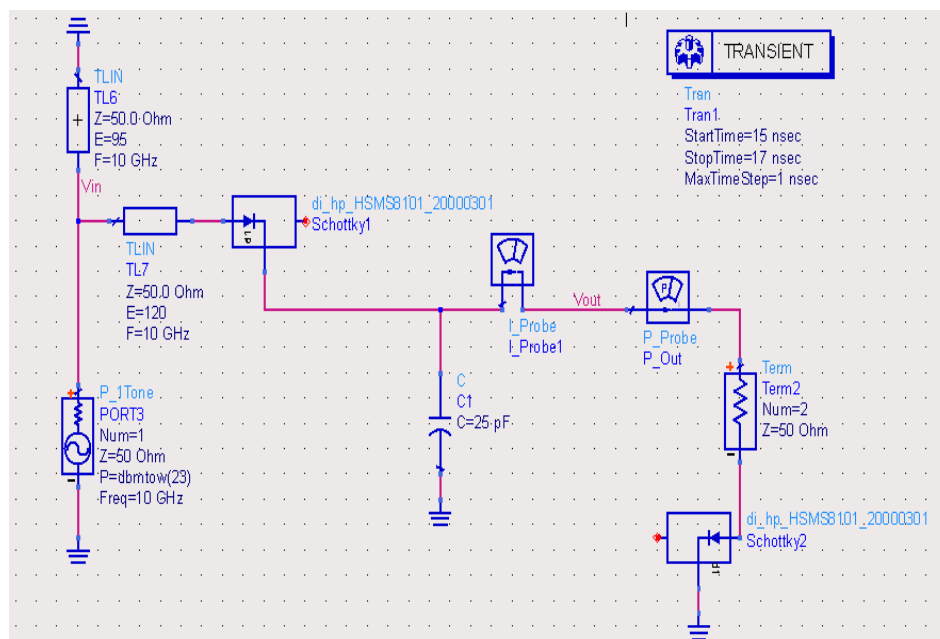
Figure 32.   ADS model of a hybrid rectenna design without LPF.

Figures 33 to 35 illustrate the output dc power produced by three different circuit designs of hybrid rectenna that were simulated in ADS.

Figure 33.　　Output power (watts) versus time for a hybrid rectenna design with a pre-LPF.

Figure 34.　　Output power (watts) versus time for a hybrid rectenna design with a post-LPF.

36

Figure 35.   Output power (watts) versus time for a hybrid rectenna design without LPF.

The simulated conversion efficiency of the three hybrid rectenna designs are given in Figure 36. The efficiency of the hybrid rectenna with post-LPF is higher than those with pre-LPF and no-LPF. In comparison to the previous results given in Figure 36, the design with post-LPF is able to convert wireless power to dc power with an efficiency of 61.2% at an input power 140 mW, but the design with pre-LPF only achieves an efficiency of 45% at the same input power.

Figure 36.   Simulated conversion efficiency of the hybrid rectennas.

3.   Full-Wave Rectenna Design

In reference [23], Chiou presented a full-wave rectenna circuit in order to obtain a more stable dc output voltage than that a half-wave rectenna of the same chip area. He demonstrated the feasibility of a rectenna with an efficiency of 53% at an incident radiation power density of 30 W/cm^2 and frequency of 35 GHz. The rectenna comprised a power-receiving linear tapered slot antenna (LTSA), a slot line (SL) to finite-width ground coplanar waveguide (FGCPW) transition, a bandpass filter (BPF), a full-wave rectifier for rf-to-dc conversion, a dc bypass capacitor, and a resistive load. The fabricated rectenna with off-chip lumped elements is depicted on Figure 37.
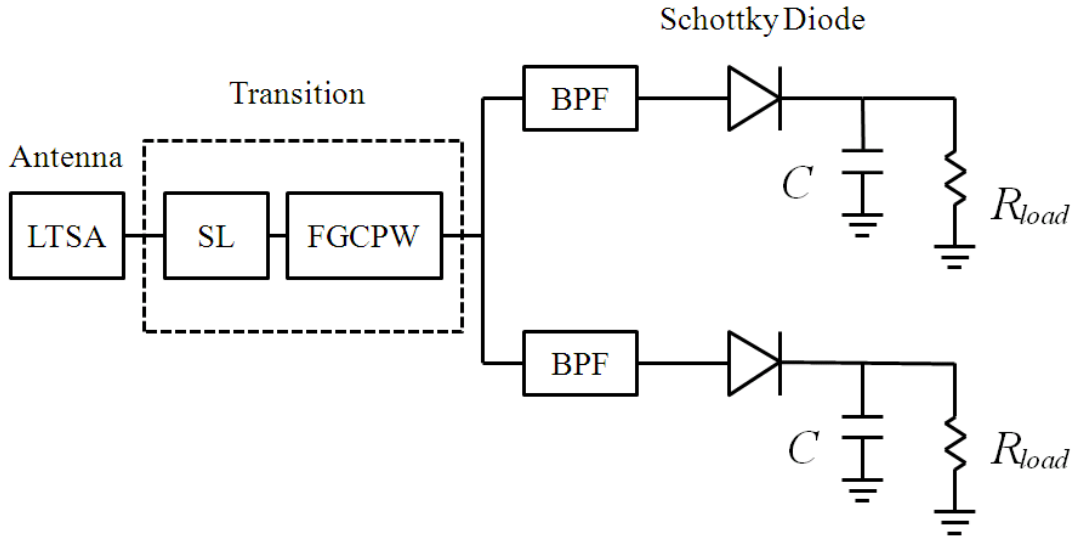
Figure 37.   Block diagram of full-wave rectifier (From [23]).

As in the previous circuit, in order to minimize the size and weight, elimination of the low-pass filter is considered. For our design, a microstrip-fed dipole will be used in place of the LTSA. It is a lighter-weight structure that can be tuned to 10 GHz, whereas the LTSA is a broadband structure. Figures 38 to 40 illustrate the three different circuit designs for a full-wave rectenna.

In the ADS model, the antenna is represented by a power source with 50 Ω impedance. The diodes are matched using shorted stubs placed the required distance from the diodes. The stub location and stub length were computed using the standard stub-matching procedure [24]. Then the ADS optimization program was used to adjust the line lengths so the output power was a maximum.
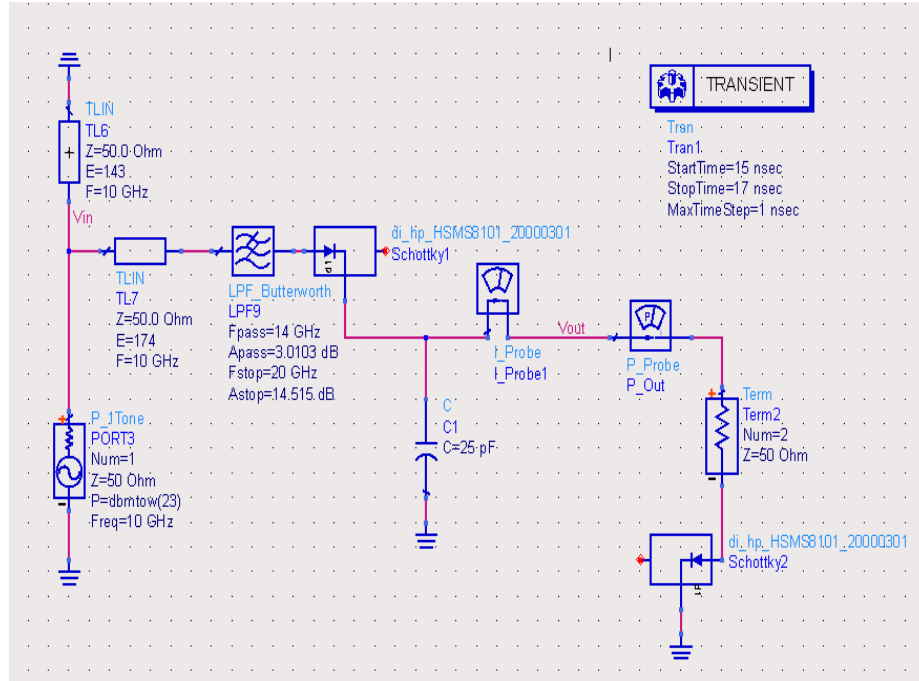
Figure 38.   ADS model of a full-wave rectenna design with a pre-LPF.

Figure 39.   ADS model of a full-wave rectenna design with a post-LPF.
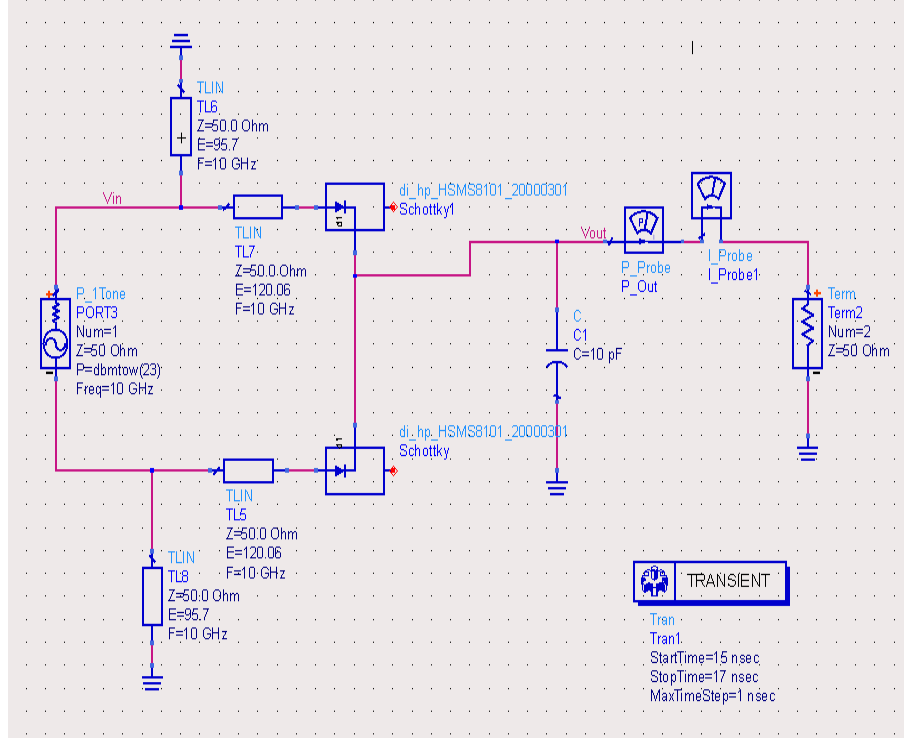
Figure 40.   ADS model of a full-wave rectenna design without LPF.

The same method used to obtain Equation (3.4) was applied to the full-wave rectenna for the discharge time. The derivative expression for the output voltage V_{out} becomes

$$V_{out} = V_P \left(1 - \frac{1}{4 f R_L C} \right). \tag{3.10}$$

Equation (3.6) and (3.10) show that the average output voltage of the full-wave rectenna can approach double the half-wave rectenna.

Figures 41 to 43 illustrate the output dc power produced by three circuit designs of the full-wave rectenna that were simulated in ADS.

41
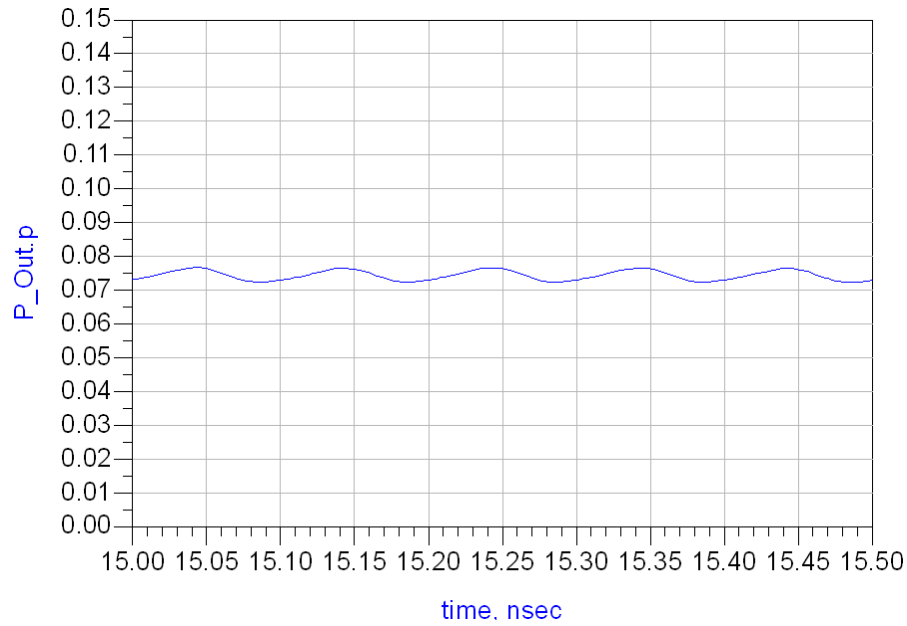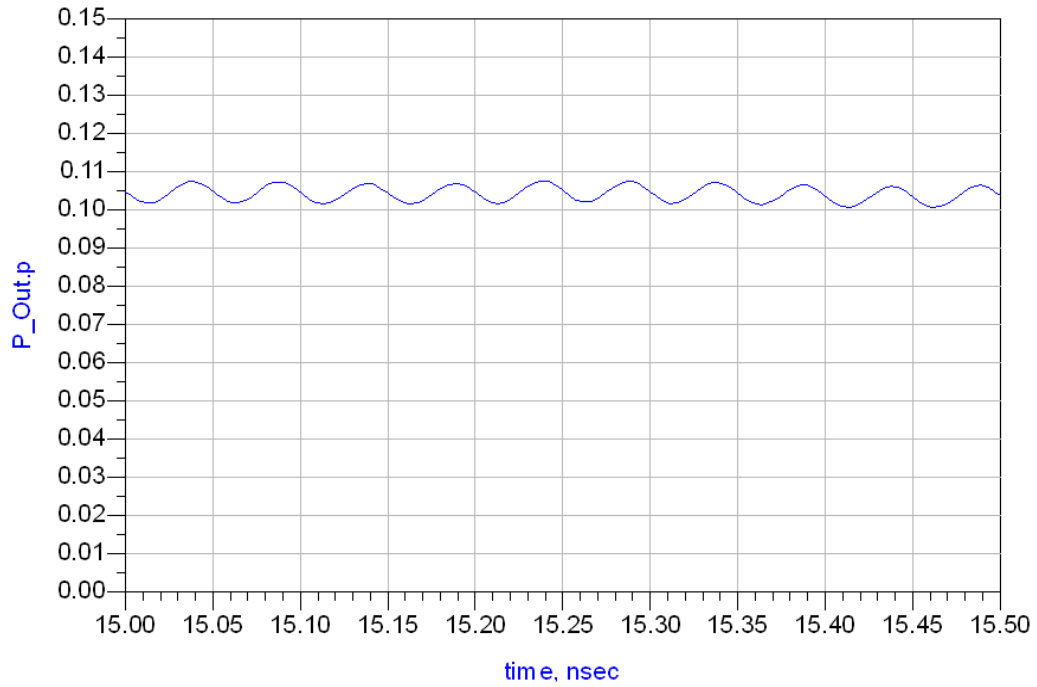
Figure 41.   Output power (watts) versus time for a full-wave rectenna design
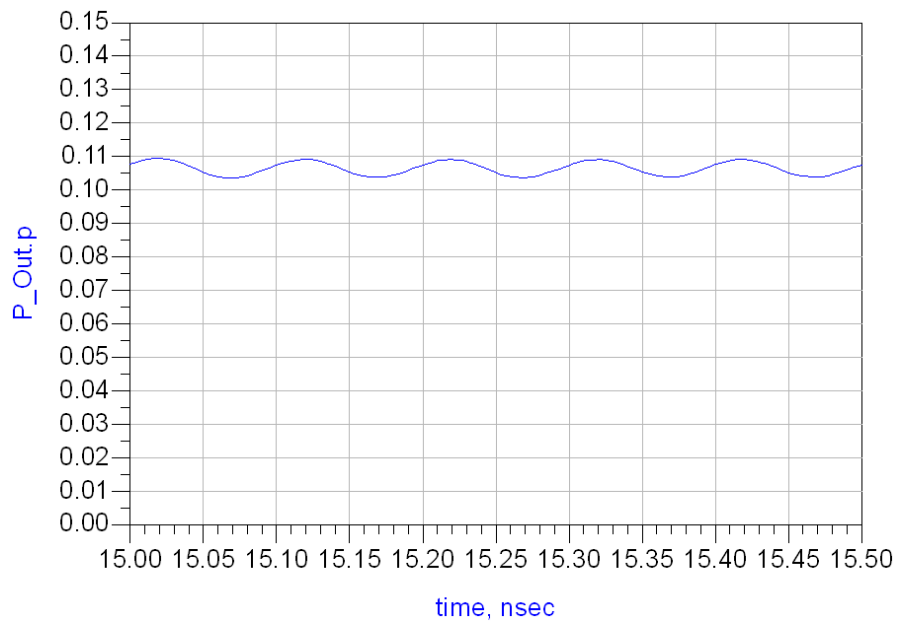with a pre-LPF.
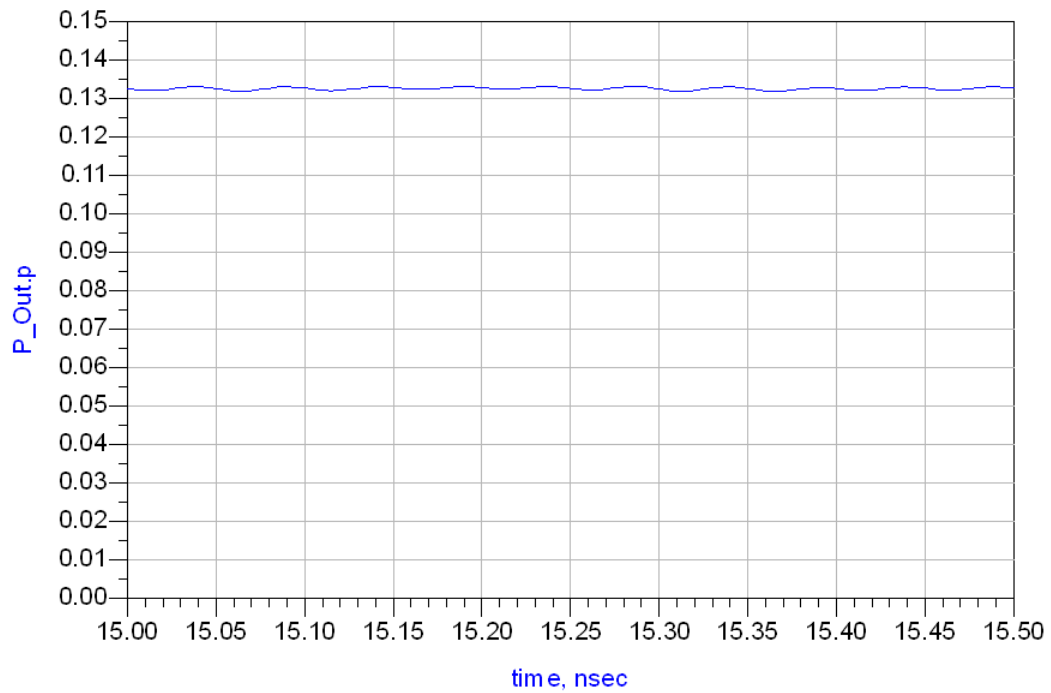
Figure 42.   Output power (watts) versus time for a full-wave rectenna design
with a post-LPF.

42
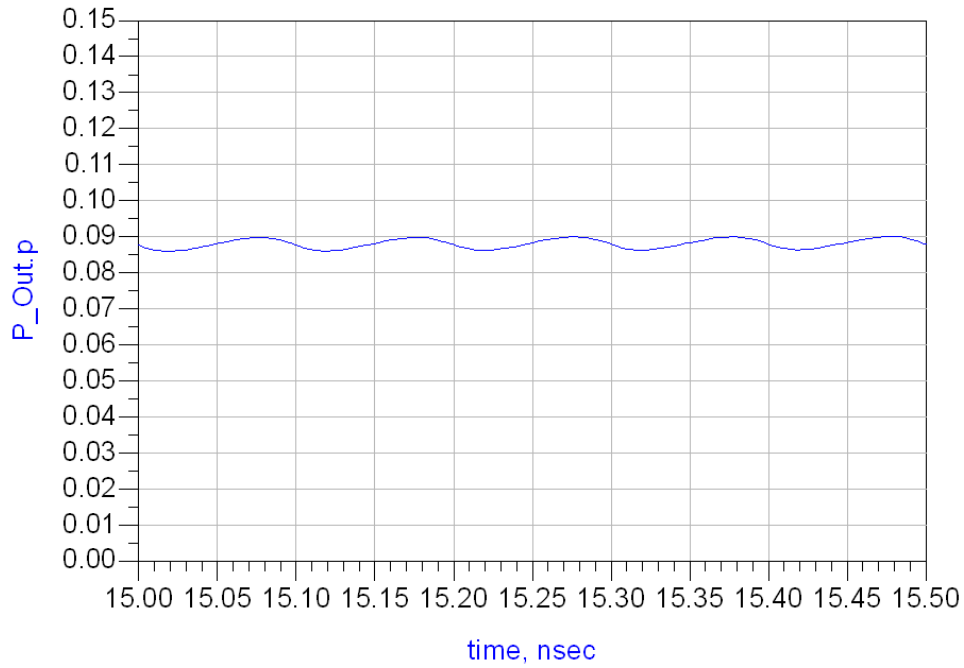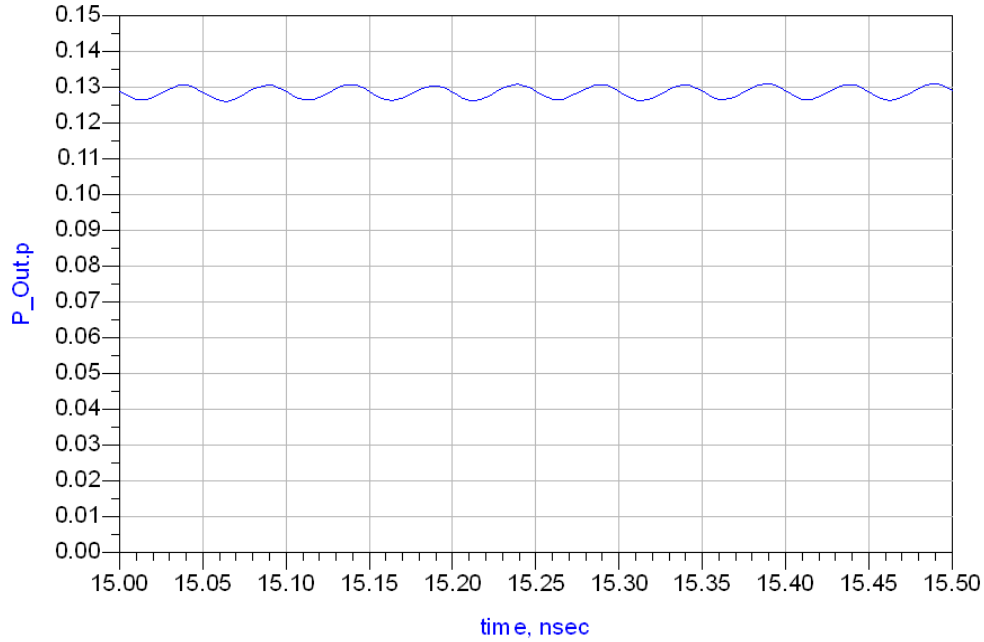
Figure 43.   Output power (watts) versus time for a full-wave rectenna design without LPF.

The simulated conversion efficiencies of the three full-wave rectenna designs are given in Figure 44. In Figure 44, the efficiency of the full-wave rectenna with post-LPF and no-LPF are the same and higher than that with pre-LPF. In comparison with the previous results in Figure 33, the design with no LPF is able to convert wireless power to dc power with an efficiency of 68.1% at an input power of 170 mW, but the design with pre-LPF only achieves an efficiency of 56.6% at the same input power.
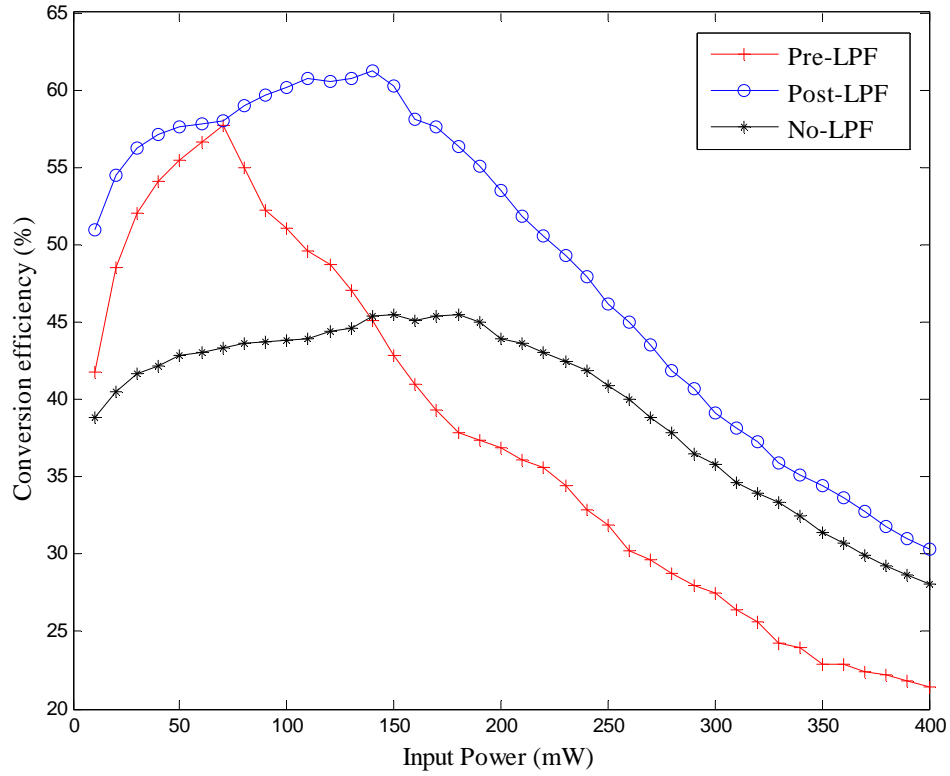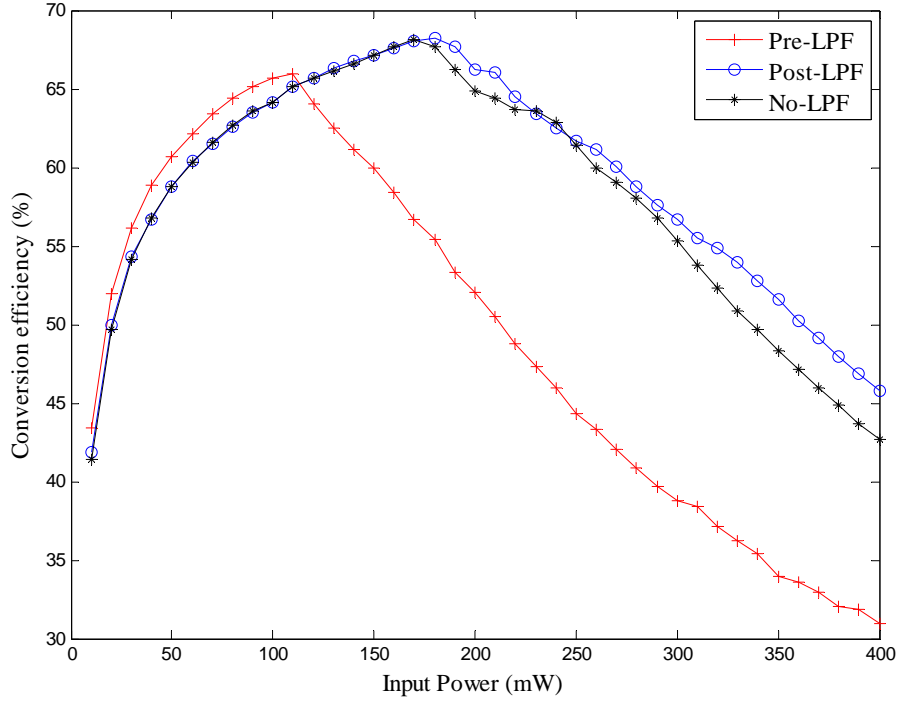
Figure 44.   Simulated conversion efficiency of full-wave rectenna using ADS with different LPF.

4.   Conclusion

Comparing previous results, we observed that the conversion efficiency of the hybrid rectenna is higher than that of the half-wave rectenna, which confirms the research conducted by Zbitou [18]. In order to hover the MAV, the full-wave rectenna with no LPF is selected to achieve the highest efficiency (68.1%) of the various rectenna designs and obtain more stable dc power than with the half-wave rectenna. The full-wave rectenna with no LPF also provides a lightweight design for the MAV application.

C.   EVALUATION OF HARMONIC FREQUENCIES

In reference [12], Hagerty reported that reflected harmonic energy from the input or output side of the diode can alter the voltage across the diode. The diode also begins to bias itself as it produces more dc current, thus moving the dc operating point of the I-V curve in a nonlinear fashion. The diode's harmonic frequency components can possibly be radiated by the antenna, causing interference with other systems. Based on the

44

properties of the diode at microwave frequencies, we simulate and analyze the radiated harmonics and dc power of different rectenna designs for an input microwave power at 10 GHz. This can be accomplished using the harmonic balance (HB), nonlinear-circuit analysis module of the ADS software.

1.   Harmonic Balance Analysis for the Half-Wave Rectenna

Figures 45 to 46 illustrate the harmonic balance of a half-wave rectenna with pre-LPF. The power in the fundamental frequency, the second through fourth harmonics, and the dc power are shown at four locations in the circuit (at the probes highlighted in the figure). These are the same cases shown in Figures 25 through 27, and their voltage and power curves were shown previously.

Figure 45.   Harmonic balance of configuration in half-wave rectenna with pre-LPF.

Figure 46.   Simulated input power, reradiated harmonic powers, and dc power (in dBm) versus frequency for the half-wave rectenna with pre-LPF.

The simulation results for the power in the harmonics at different nodes in the circuit are given in Table 3. Pbf is the power before the low-pass filter, Paf is the power after the low-pass filter, Pbs is the power after the Schottky diode, and Pout is the power at the output of the circuit. The unit is dBm. Examination of the results in Table 3 shows that the harmonics reflected by diode are eliminated by the low-pass filter. The 80 pF capacitor performs as a dc pass filter to eliminate any leakage of 10 GHz signal. We confirm the above simulation by comparing the dc power of the harmonic balance simulation with that of the transient simulation, and found that the two results agree.

46

Harmonic balance analysis data for fundamental frequency of 10 GHz (Pin=23 dBm)					
Node	0 Hz	10 GHz	20 GHz	30 GHz	40 GHz
Pbf (dBm)	-34.302	22.887	-13.708	-51.469	-75.358
Paf (dBm)	-34.302	22.887	-13.708	-51.469	-75.358
Pas (dBm)	19.634	-26.804	-45.813	-74.595	-86.818
Pout (dBm)	19.634	-26.804	-45.813	-74.595	-86.818

Table 3.   Harmonic balance data for the half-wave rectenna with pre-LPF.

Figures 47 to 48 illustrate the harmonic balance model of the half-wave rectenna with post-LPF and the power probes at different nodes in the circuit.

Figure 47.   Harmonic balance simulation configuration for the half-wave rectenna with post-LPF.
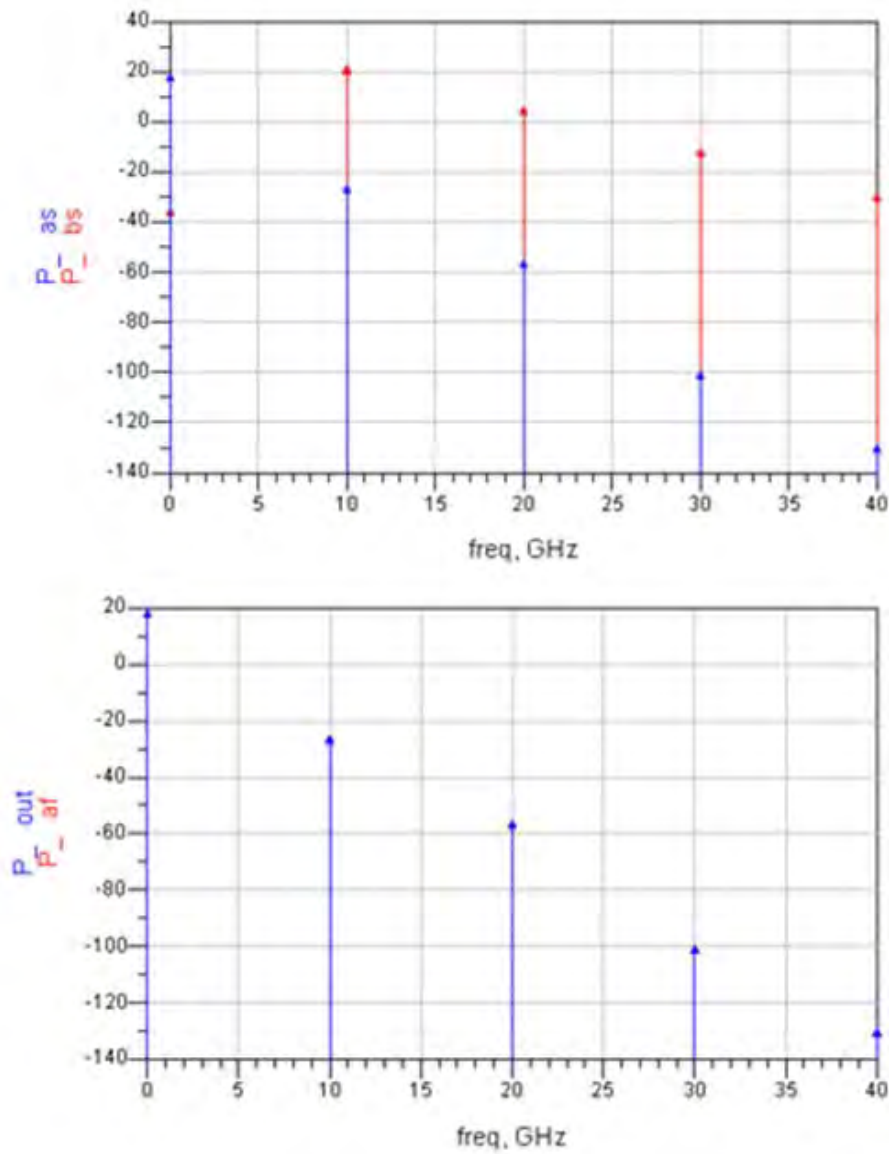
Figure 48.   Simulated input power, reradiated harmonic powers, and dc power (in dBm) versus frequency for the half-wave rectenna with post-LPF.

Table 4 is a list of the power in the harmonics at different nodes in the circuit shown in Figure 45. Pbs is the power before the Schottky diode, Pas is the power after the diode, Paf is the power after the low-pass filter, and Pout is the power at the output. A comparison of the results in Table 4 shows that the highest harmonic reflected by diode and reradiated toward antenna was about 6 dBm at 20 GHz; the third and forth harmonics were negligible for this design. The low-pass filter and 80 pF capacitor reduced the

harmonics produced by diode and produced stable dc power. We confirmed the above simulation by comparing the dc power of harmonic balance simulation with the transient simulation, and the results agree.

Harmonic balance analysis data for fundamental frequency of 10 GHz (Pin=23 dBm)					
Node	0 Hz	10 GHz	20 GHz	30 GHz	40 GHz
Pbs (dBm)	-34.555	22.342	5.914	-10.423	-28.589
Pas (dBm)	19.381	-25.154	-55.312	-99.631	-129.019
Paf (dBm)	19.381	-25.154	-55.312	-99.631	-129.019
Pout (dBm)	19.381	-25.154	-55.312	-99.631	-129.019

Table 4.   Harmonic balance data for the half-wave rectenna with post-LPF.

Figures 49 to 50 illustrate the harmonic balance of the half-wave rectenna without LPF and the power in the fundamental frequency, harmonics, and dc at different nodes in the circuit.
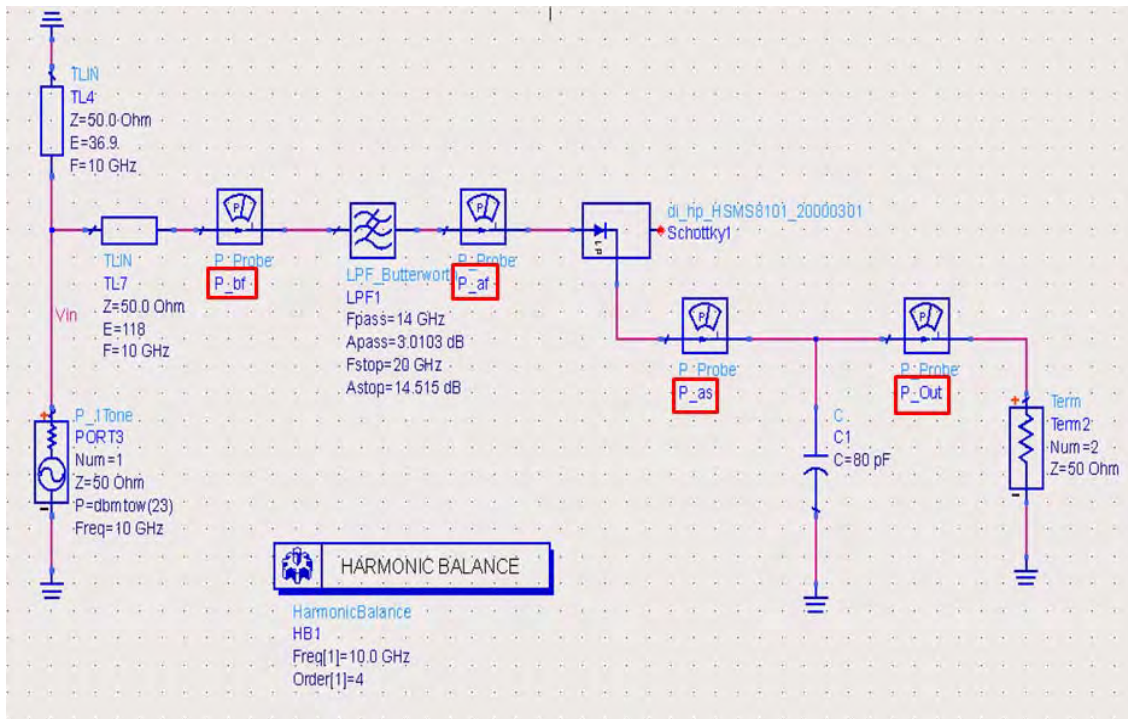

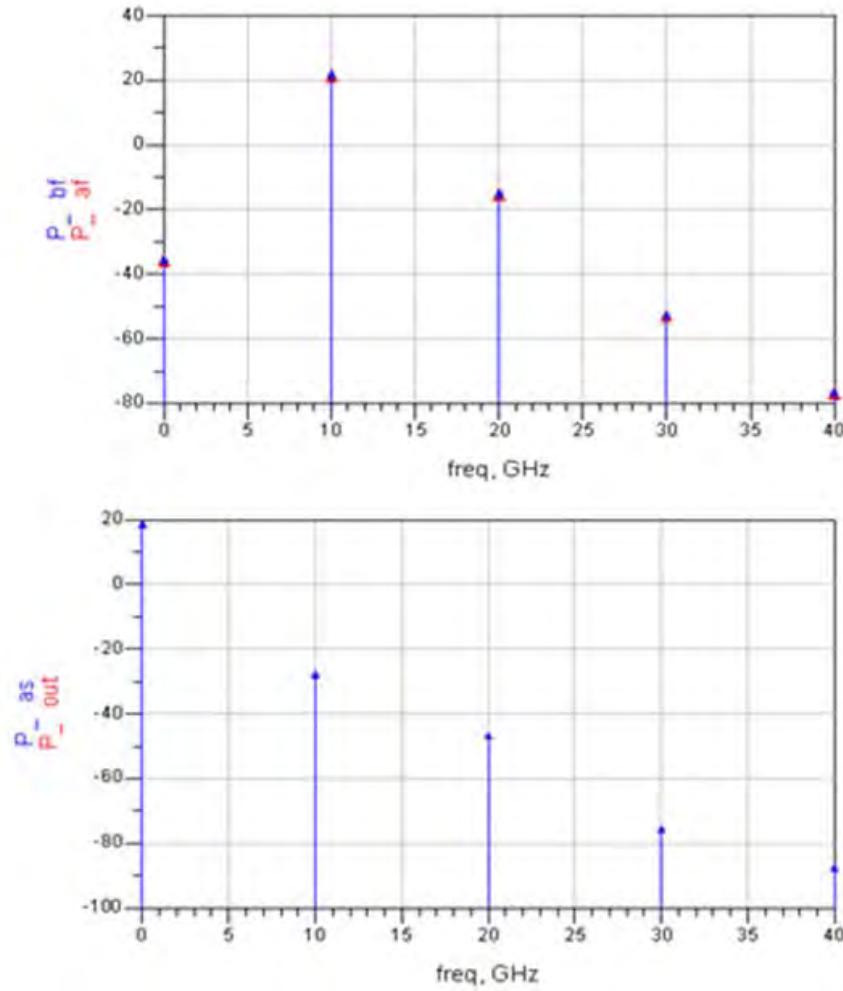Figure 49.   Harmonic balance simulation configuration for the half-wave rectenna without LPF.

Figure 50.   Simulated input power, reradiated harmonic power, and dc power
(in dBm) versus frequency for the half-wave rectenna without LPF.

Table 5 is a list of the power in the harmonics at different nodes in the circuit. Pbs is the power before the Schottky diode, Pas is the power after the diode, and Pout is the power at the output. In comparison to the results in Table 5, the highest harmonic reflected by diode and reradiated toward antenna was about 5 dBm at 20 GHz, but the third and fourth harmonics were small and acceptable for our design. The 80 pF capacitor reduced the harmonics produced by diode and produced stable dc power. We confirmed the above simulation by comparing the dc power of the harmonic balance with the transient simulation, and the results agree.

Harmonic balance analysis data for fundamental frequency of 10 GHz (Pin=23 dBm)					
Node	0 Hz	10 GHz	20 GHz	30 GHz	40 GHz
Pbs (dBm)	-35.061	21.128	4.968	-3.422	-22.986
Pas (dBm)	18.876	-27.815	-44.730	-59.540	-78.615
Pout (dBm)	18.876	-27.815	-44.730	-59.540	-78.615

Table 5.   Harmonic-balance data for the half-wave rectenna without LPF.

2.   Harmonic Balance Analysis for the Full-Wave Rectenna

Figures 51 to 52 illustrate the harmonic balance of a full-wave rectenna with pre-LPF and the power in the fundamental frequency, harmonics, and dc at different nodes in the circuit.
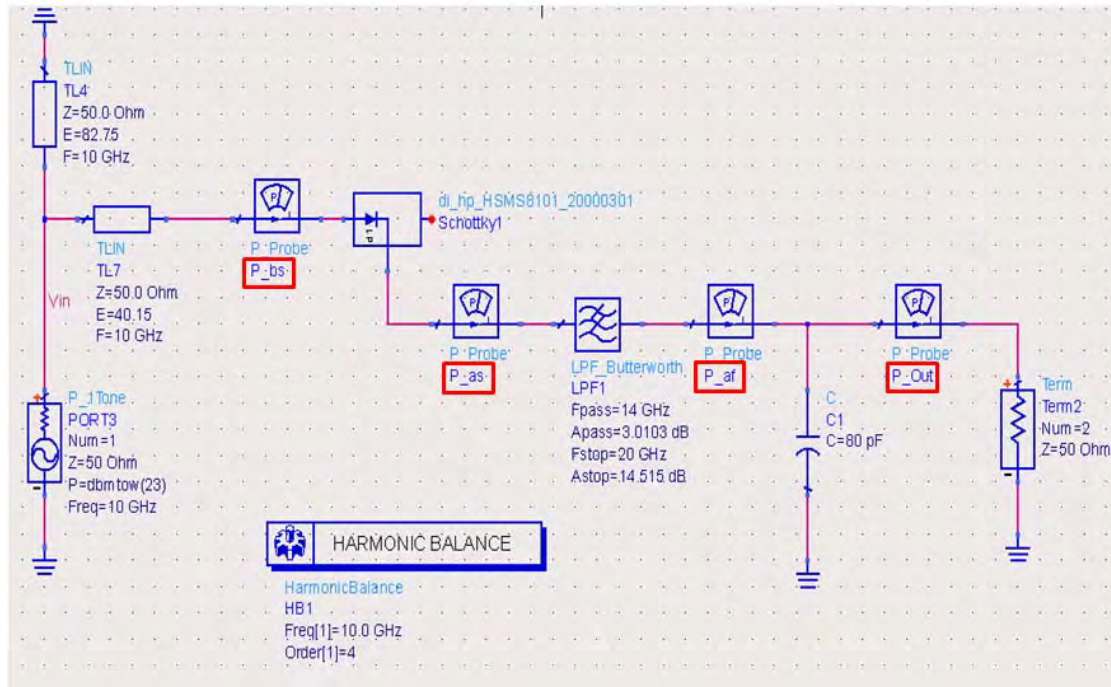

Figure 51.   Harmonic-balance simulation configuration for the full-wave rectenna with pre-LPF.

51

Figure 52.   Simulated input power, reradiated harmonic power, and dc power
(in dBm) versus frequency in full-wave rectenna with pre-LPF.

The power in the harmonics at different nodes in circuit is given in Table 6. Pbf is

the power before the lowpass filter, Paf is the power after LPF, Pas is the power after the

Schottky diode, Pfin is the combined power after the two diodes and Pout is the power at

the output of the circuit. The harmonics reflected by diode were eliminated by the low-pass filter. The full-wave architecture essentially eliminates the frequencies of 10 GHz and 30 GHz at the output. The 10 pF capacitor performs as a dc pass filter to eliminate the frequencies 20 GHz and 40 GHz. These simulation results were compared to the transient simulation, and the results agree.

Harmonic balance analysis data for fundamental frequency of 10 GHz (Pin=23 dBm)					
Node	0 Hz	10 GHz	20 GHz	30 GHz	40 GHz
Pbf (dBm)	-40.149	19.934	-145.177	-59.528	-188.391
Paf (dBm)	-40.149	19.934	-140.204	-59.528	-172.270
Pas (dBm)	16.797	-145.791	-23.490	-170.867	-63.062
Pfin (dBm)	19.808	-304.622	-20.480	-313.664	-60.051
Pout (dBm)	19.808	-326.624	-20.480	-330.596	-60.051

Table 6.   Harmonic balance data for the full-wave rectenna with pre-LPF.

Figures 53 to 54 illustrate the harmonic balance of the full-wave rectenna with post-LPF and the power in the fundamental, harmonics, and dc at different nodes in circuit.
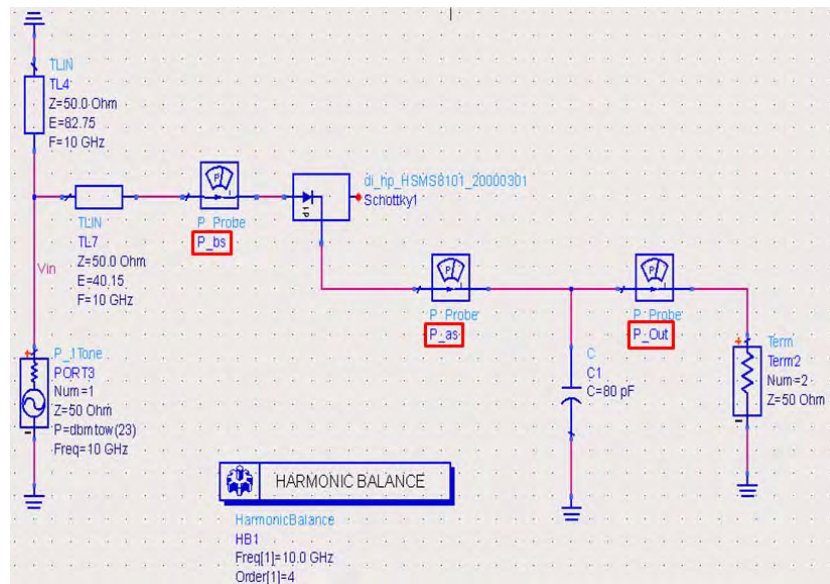
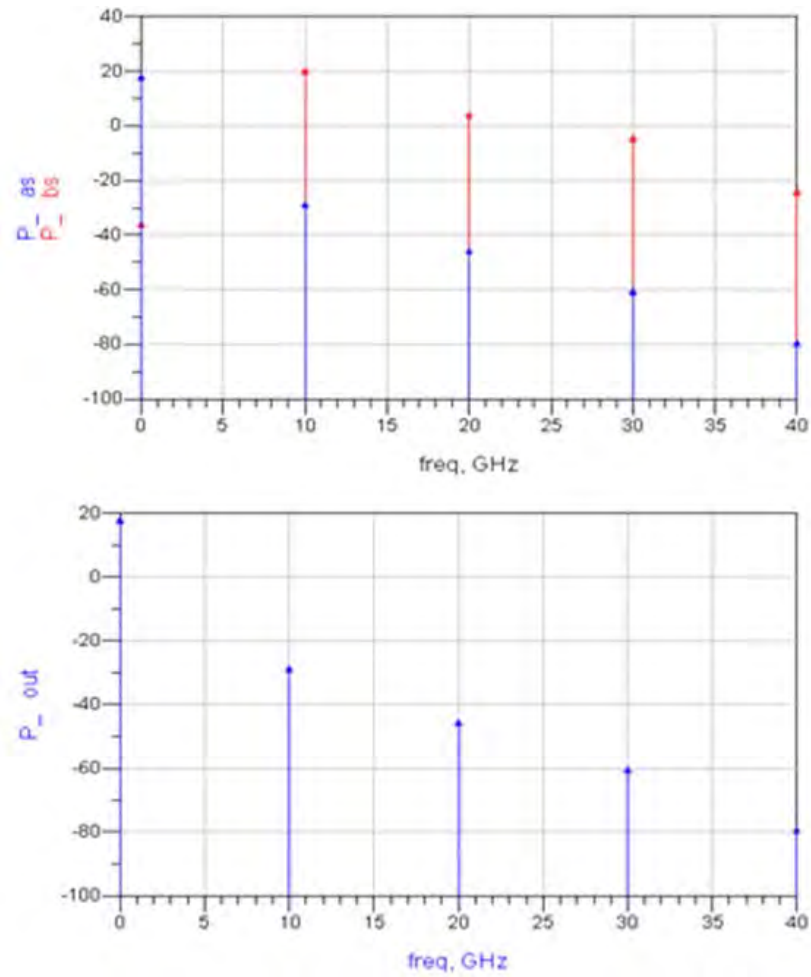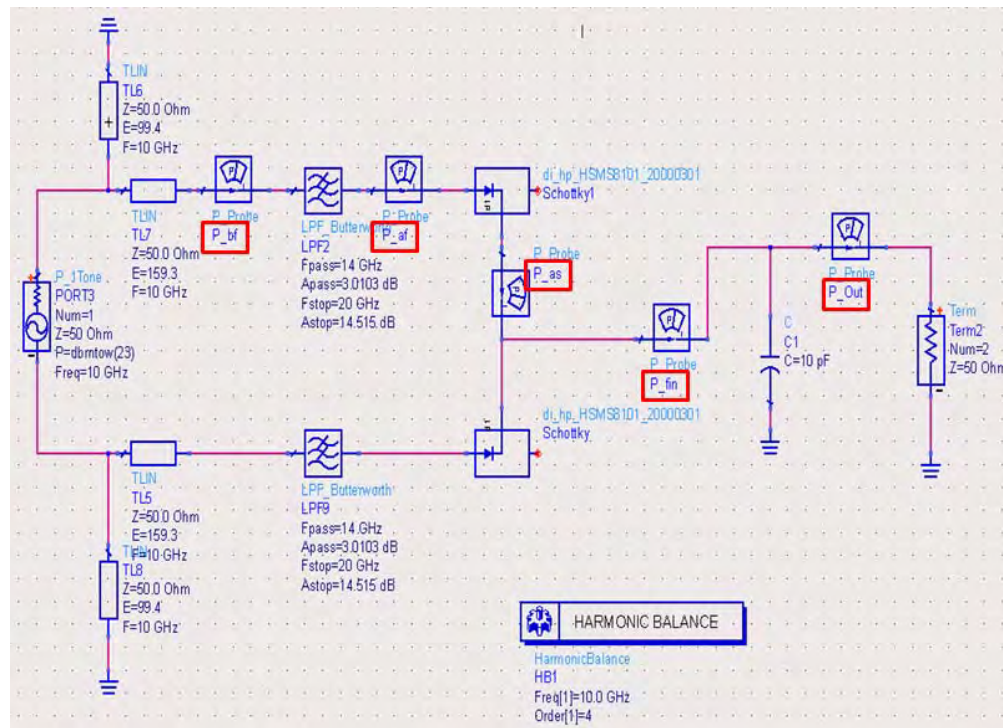Figure 53.	Harmonic-balance simulation configuration for the full-wave rectenna with post-LPF.

Figure 54.   Simulated input power, reradiated harmonic power, and dc power (in dBm) versus frequency for the full-wave rectenna with post-LPF.

The power in the harmonics at different nodes in the circuit is given in Table 7, where Pbs is the power before the Schottky diode, Pas is the power after the diode, Pbf is the combined power of the two diodes and measured before the LPF, Pfin is the power after LPF, and Pout is the power at output. In comparison to the results of Table 7, the highest harmonic power reflected by the diode was -2 dBm at 30 GHz and there was negligible power at 10 GHz after the diode for the full-wave design. The full-wave architecture also eliminates the frequency of 30 GHz after the diode. The 10 pF capacitor performs as dc pass filter to eliminate the frequency of 20 GHz and 40 GHz. The simulation results were compared to the transient simulation, and the results agree with each other.

Harmonic balance analysis data for fundamental frequency of 10 GHz (Pin=23 dBm)					
Node	0 Hz	10 GHz	20 GHz	30 GHz	40 GHz
Pbs (dBm)	-39.176	19.839	-144.086	-2.080	-169.107
Pas (dBm)	17.770	-136.007	-38.575	-142.487	-106.223
Pbf (dBm)	20.781	-300.027	-35.564	-295.822	-103.212
Pfin (dBm)	20.781	-335.853	-35.564	-336.802	-103.212
Pout (dBm)	20.781	-317.919	-35.564	-352.415	-103.212

Table 7.   Harmonic-balance data for the full-wave rectenna with post-LPF.

Figures 55 to 56 illustrate the harmonic balance of full-wave rectenna without LPF and the power in the fundamental frequency, harmonics, and dc at different nodes in circuit.

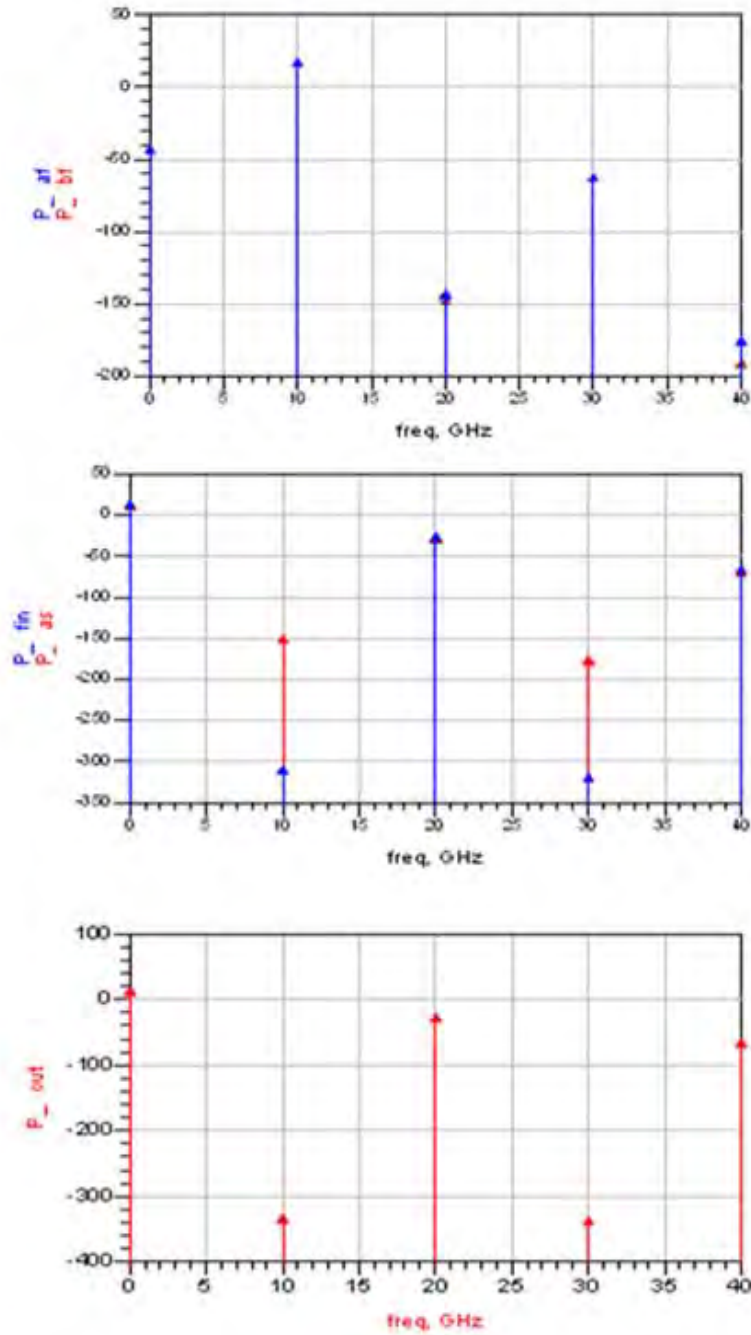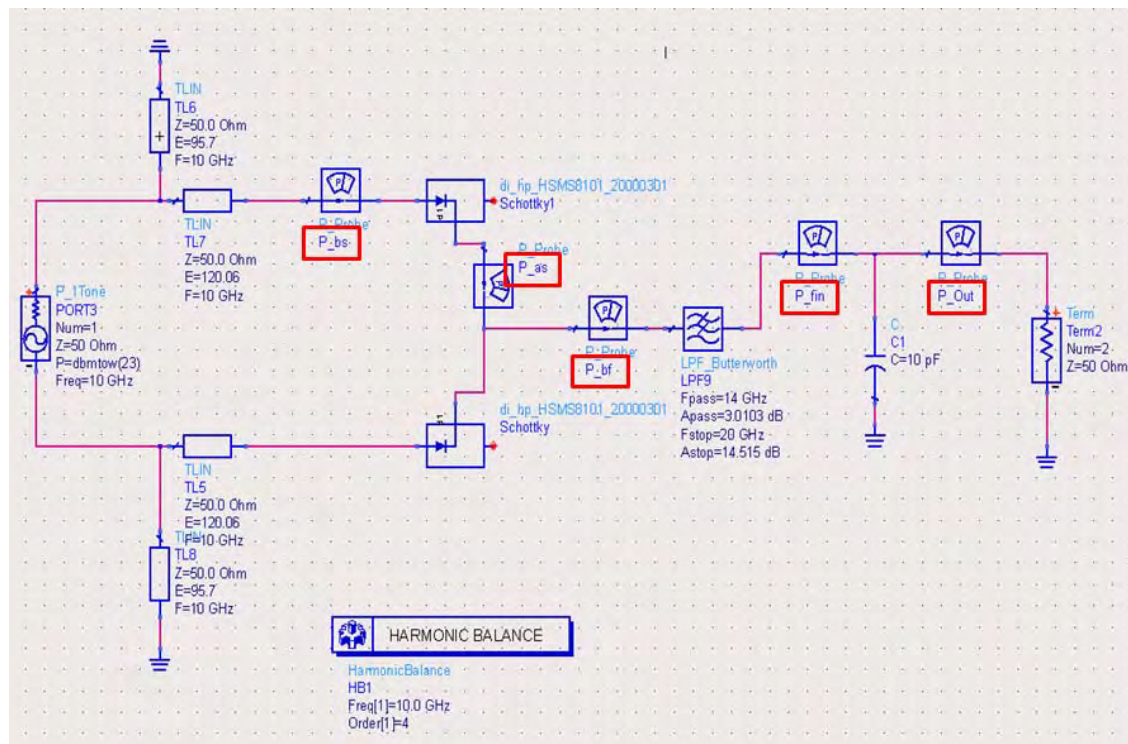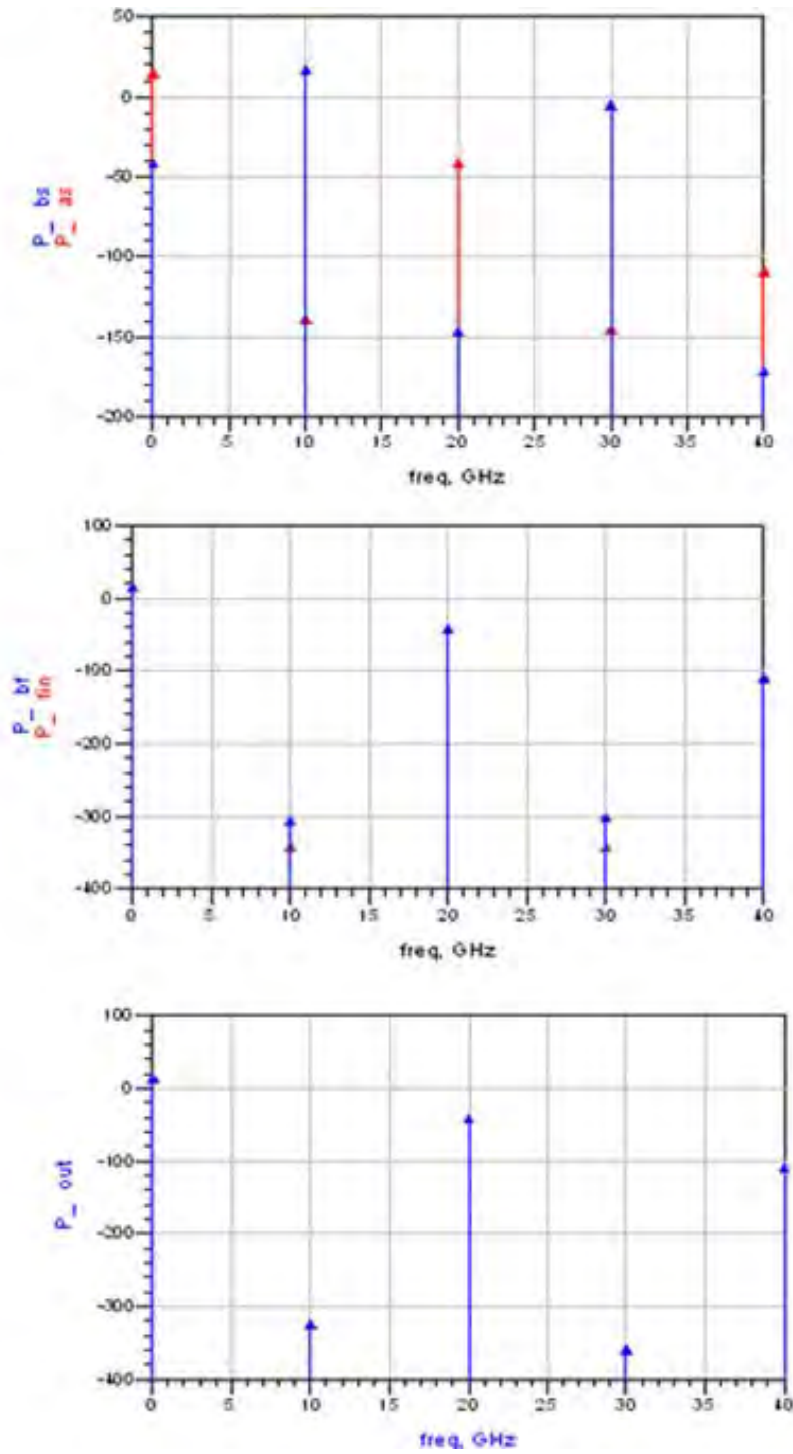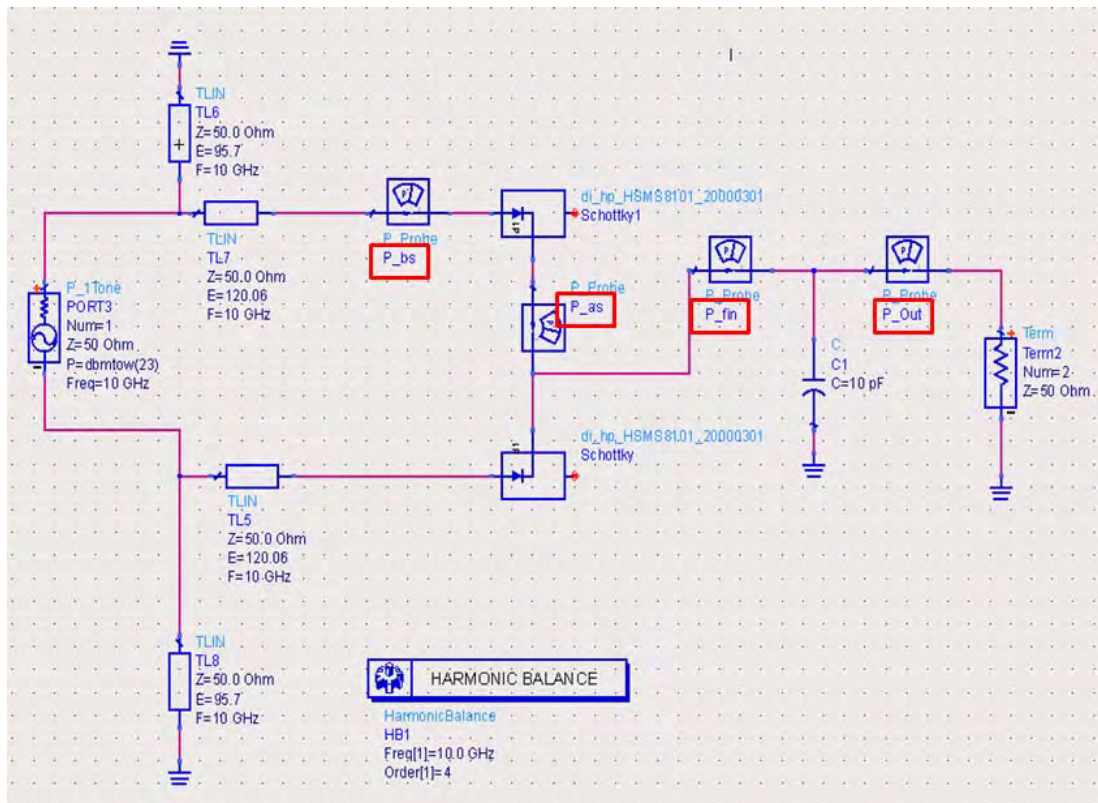Figure 55.   Harmonic-balance simulation configuration for the full-wave rectenna without LPF.
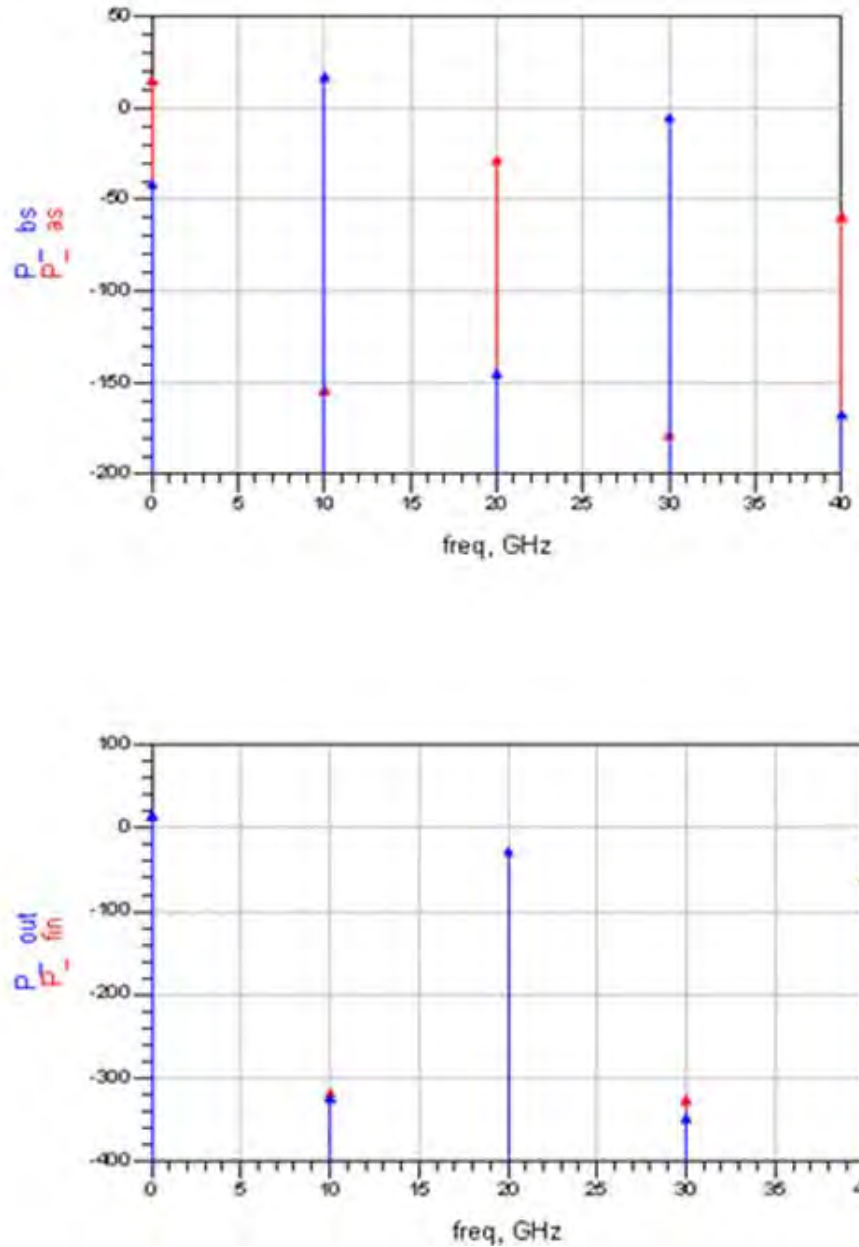
Figure 56.   Simulated input power, reradiated harmonic power, and dc power (in dBm) versus frequency for the full-wave rectenna without LPF.

The simulation results for the power in the harmonics at different nodes in the circuit are given in Table 8. Pbs is the power before the Schottky diode, Pas is the power after the diode, Pfin is the combined power of the two diodes before the capacitor, and Pout is the power at the output. In comparison to the results in Table 8, the highest harmonic power generated by the diode was -3 dBm at 30 GHz and there was negligible

58

fundamental power at the output for the full-wave design. The 10 pF capacitor performs as a dc pass filter to eliminate the frequency of 20 GHz and 40 GHz. The simulation was compared to the transient simulation, and the results agree.

Harmonic balance analysis data for fundamental frequency of 10 GHz (Pin=23 dBm)					
Node	0 Hz	10 GHz	20 GHz	30 GHz	40 GHz
Pbs (dBm)	-39.277	19.824	-142.325	-3.127	-164.700
Pas (dBm)	17.670	-151.310	-26.147	-175.864	-56.734
Pfin (dBm)	20.680	-312.757	-23.137	-321.039	-53.723
Pout (dBm)	20.680	-318.761	-23.137	-343.172	-53.723

Table 8.　　Harmonic-balance data for the full-wave rectenna without LPF.

3.　　Findings

After comparing the three half-wave rectenna designs, we conclude that the half-wave rectenna with pre-LPF has better performance due to its limitation of harmonics back toward the antenna and slightly higher efficiency, albeit not much. The half-wave rectenna only converts at best half of the microwave energy, but the full-wave rectenna ideally converts all power, due to its architecture. We also observe that the full-wave rectenna without LFP converts more dc power than other designs and the full-wave rectifier design eliminates the fundamental frequency and third harmonic frequency at the output. In order to have a lightweight rectenna, the full-wave rectenna without LFP is selected. In the next chapter, we discuss the impedance of the full-wave rectification rectenna without LPF and optimize the impedance matching unit.

THIS PAGE INTENTIONALLY LEFT BLANK

IV.   RECTENNA IMPLEMENTATION

A.   RECTENNA IMPEDANCE DESIGN

Chapter III presented the simulation results for several different rectenna designs. We conclude that the full-wave rectenna without LPF meets the MAV requirement because of its higher conversion efficiency and constant output power. This chapter discusses the impedance matching of the rectenna and the circuit design and layout.

1.   Full-Wave Rectenna Design

The full-wave rectenna design with the final optimized circuit and dielectric material is shown in Figure 57. The simulated output dc power, voltage, and current of full-wave rectenna are shown in Figure 58. The output power of the rectenna is 131 mW for an input power of 23 dBm, and the voltage oscillates from 2.55 V to 2.53 V.
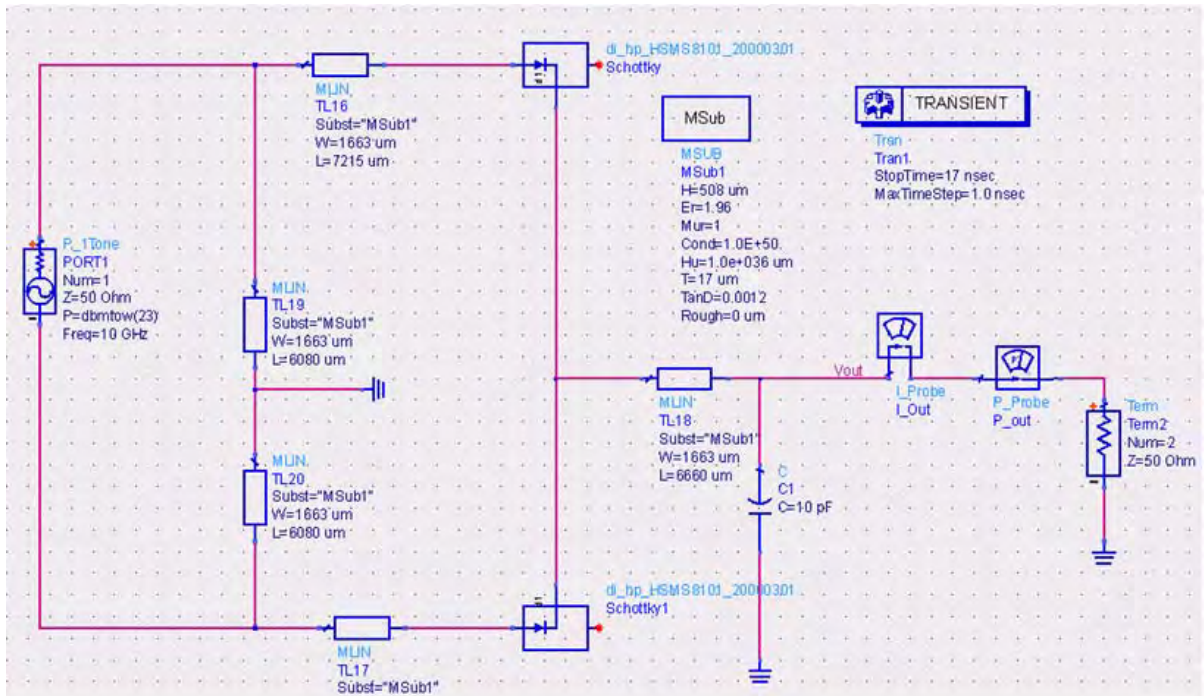
Figure 57.   Final circuit design of full-wave rectification rectenna.
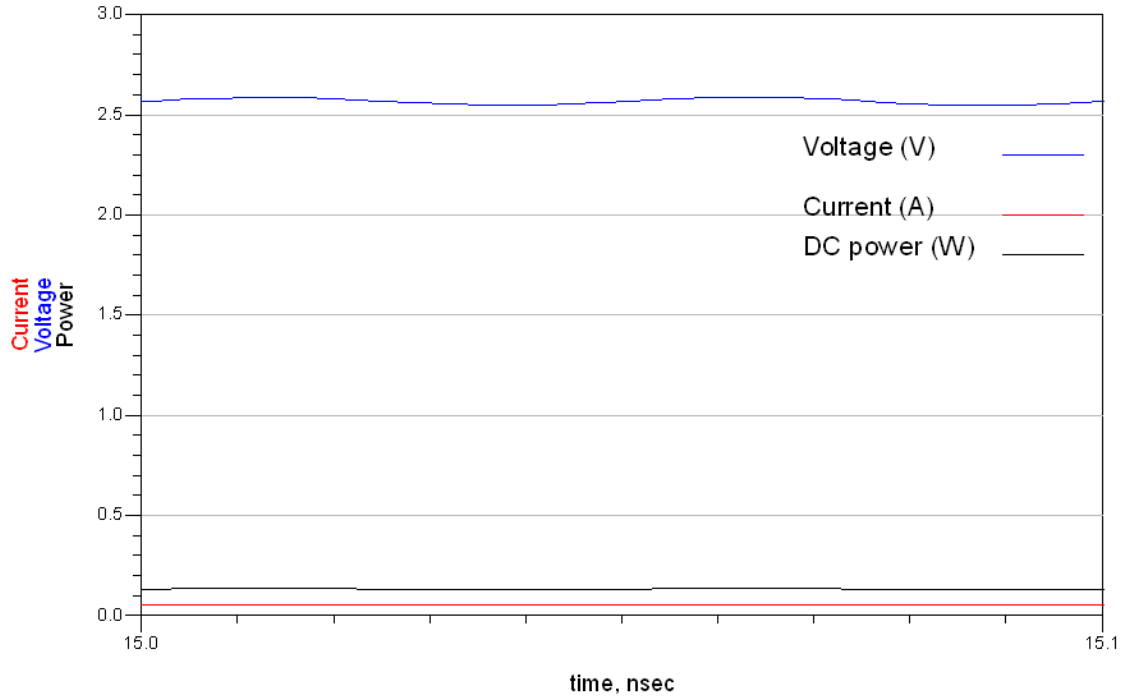
Figure 58.   Simulated output power, voltage, and current-versus-time for the
full-wave rectenna with a 23 dBm input.

2.   Performance of Full-Wave Rectenna Impedance Design

The simulated conversion efficiency of the full-wave rectenna as a function of input power is shown in Figure 59. The full-wave design is able to convert microwave power to dc power with an efficiency of 65.9% at an input power of 200 mW. The simulated output power of the full-wave rectenna design is shown in Figure 60. The full-wave design is able to produce 132 mW at an input power of 200 mW. In addition, the full-wave input–output characteristic is nearly linear, from 20 mW to 200 mW. From 200 mW to 400 mW of input power, the output begins to saturate. As a result, we prefer using the full-wave rectenna design for MAV application at an input power of 200 mW because it achieves the highest efficiency. However, to obtain this high power output requires a very large power density at the antenna, as observed in Figure 19.
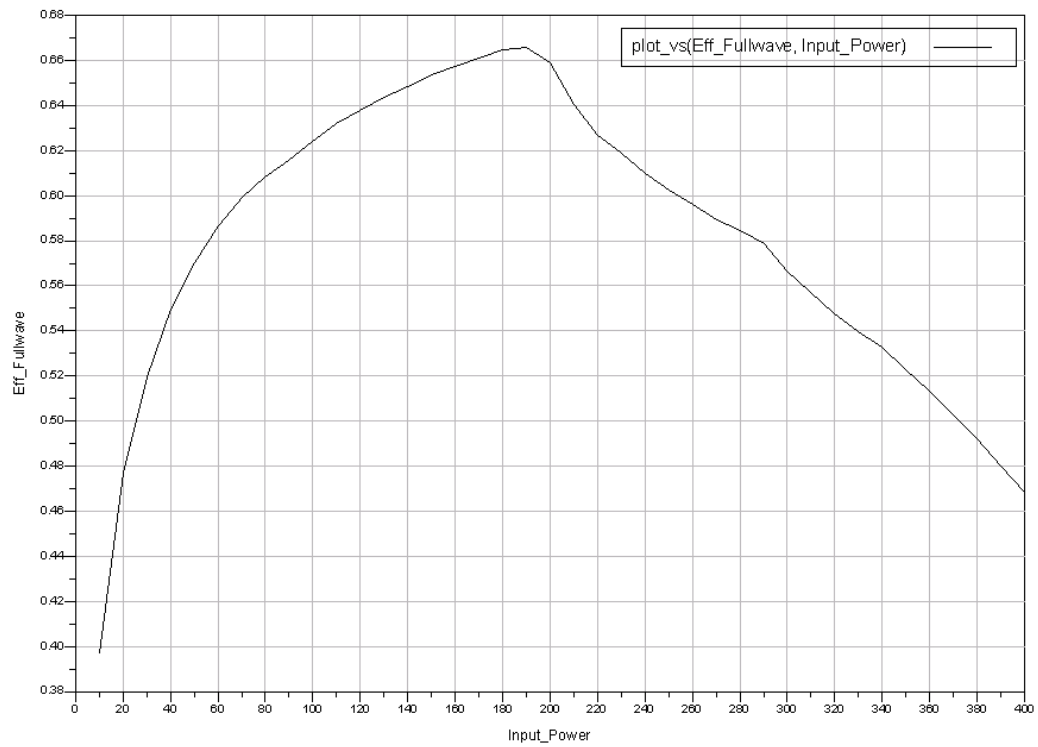
Figure 59.   Conversion efficiency of final full-wave rectenna design.
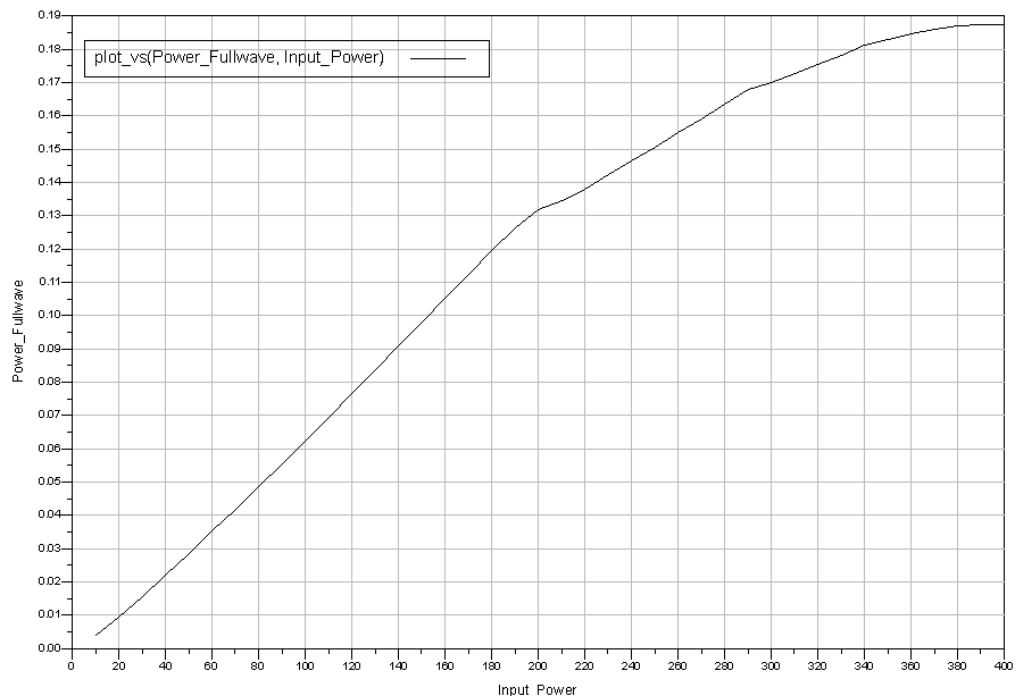
Figure 60.   Output power (watts) of final full-wave rectenna design.

63

B.   CIRCUIT LAYOUT AND TUNING

1.   Circuit Design Layout

The final circuit-design layout is shown in Figure 61. In Figure 61, the full-wave rectenna includes a matching unit, two diodes, and one capacitor. Based on the ADS simulation, the HSMS 8101 has an S_{22} characteristic impedance of 4.7 + j40 Ω. In order to have a compact circuit design to reduce the size and weight of the printed circuit board (PCB), we bend the impedance-matching unit. The length of ℓ and d are the same values as those in the ADS model in Figure 57. The calculation of the length of L_0 is discussed in the next section. For lightweight design, we select a dielectric constant of 1.96 for the substrate. The properties of the dielectric material are listed in Table 9.
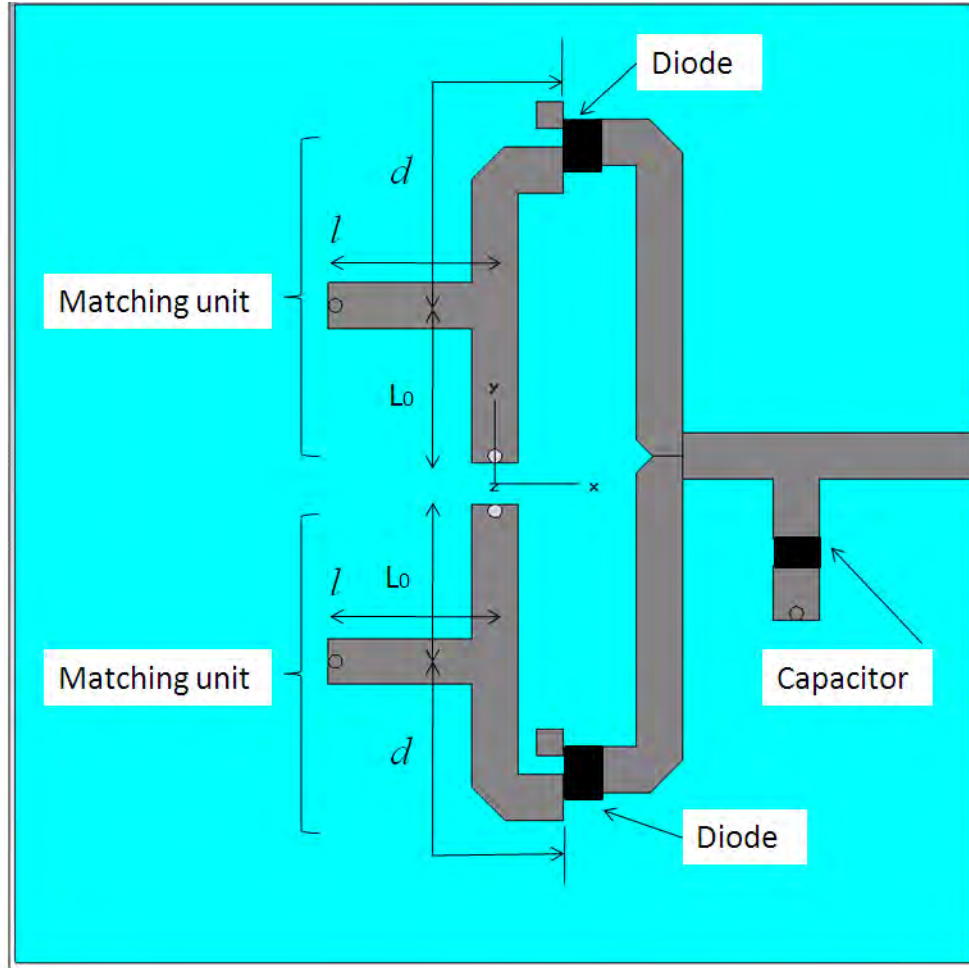
Figure 61.   Final circuit layout of the full-wave rectenna modeled in CST.

Dielectric Material	Duroid 5880LZ from Rogers Corporation
Dielectric Constant ε_r	1.96 ± 0.04
Loss Tangent, $\tan \delta$	0.0019 @ 10 GHz
Substrate Height, h	0.508 mm microstrip circuit
Copper Thickness	0.5 oz or 17 μm

Table 9.　　　Properties of Rogers Duroid 5880LZ.

2.　　　Calculation of the Matching Unit

Figure 62 shows the portion of the circuit between an antenna terminal and the diode. As seen in Figure 61, the circuit occurs at both dipole terminals. When a sinusoidal voltage is applied at the terminals, one diode will conduct, appearing as a complex impedance. The values of ℓ and d have been chosen to match the conducting diode to the 50 Ω characteristic impedance of the line. This was done using the ADS parameter sweep.

In order for the dipole to be matched at the conducting diode side, the other side must present an open circuit at the antenna terminal. Therefore L_0 must be chosen so that the combination of the open circuit at the diode (d) and its matching stub (ℓ) present an open circuit at the antenna terminal.
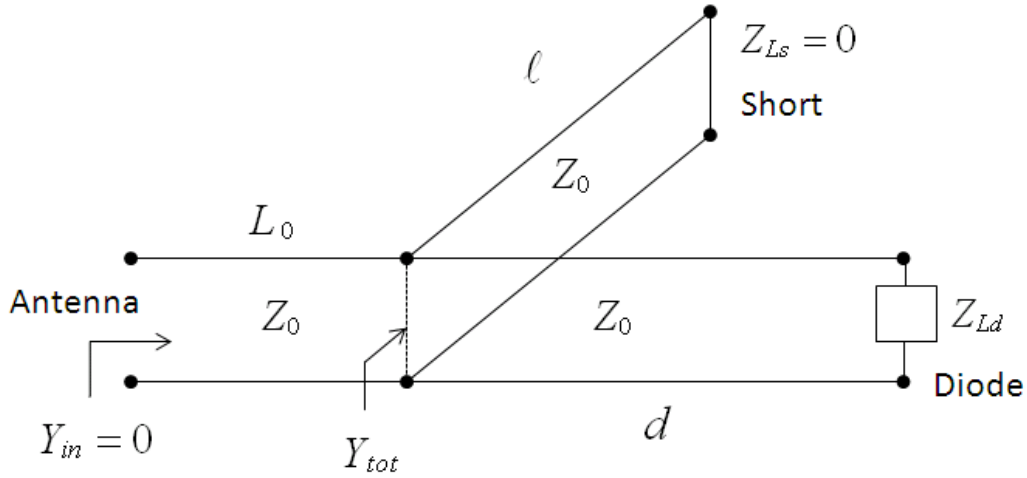
Figure 62.   Circuit diagram showing the stub position.

The impedance of the shorted transmission line ℓ at the junction can expressed as

$$Z_{ins} = Z_0 \frac{Z_{Ls} + jZ_0 \tan(\beta\ell)}{Z_0 + jZ_{Ls} \tan(\beta\ell)} = jZ_0 \tan(\beta\ell) \tag{4.1}$$

and the admittance is

$$Y_{ins} = \frac{1}{Z_{ins}} = \frac{1}{jZ_0 \tan(\beta\ell)} \tag{4.2}$$

where Z_0 is 50 Ω and Z_{Ls} is approximately 0 Ω. In addition, the impedance of the transmission line d at the junction can be expressed as

$$Z_{ind} = Z_0 \frac{Z_{Ld} + jZ_0 \tan(\beta d)}{Z_0 + jZ_{Ld} \tan(\beta d)} = \frac{Z_0}{j \tan(\beta d)} \tag{4.3}$$

where

$$Z_{Ld} = \begin{cases} 4.7 + j40 & \text{conducting} \\ \infty & \text{nonconducting} \end{cases} \tag{4.4}$$

and its admittance at the junction is

$$Y_{ind} = \frac{1}{Z_{ind}} = \frac{j \tan(\beta d)}{Z_0}. \tag{4.5}$$

66

The total admittance at the junction is

$$Y_{tot} = Y_{ins} + Y_{ind} = \frac{-j}{Z_0 \tan(\beta \ell)} + \frac{j \tan(\beta d)}{Z_0}. \tag{4.6}$$

The impedance looking into the junction must be transformed through a distance L_0.

$$Z_{in} = Z_0 \frac{Z_{tot} + jZ_0 \tan(\beta L_0)}{Z_0 + jZ_{tot} \tan(\beta L_0)} = \frac{1}{y_0} \frac{1 + jy_{tot} \tan(\beta L_0)}{y_{tot} + j \tan(\beta L_0)} \tag{4.7}$$

where $y_{tot} = \dfrac{Y_{tot}}{Y_0}$. Therefore

$$Y_{in} = \frac{1}{Z_{in}} = \frac{y_{tot} + j \tan(\beta L_0)}{1 + jy_{tot} \tan(\beta L_0)}. \tag{4.8}$$

The maximum power from the antenna occurs when Y_{in} equals to 0, therefore

$$y_{tot} + j \tan(\beta L_0) = 0 \tag{4.9}$$

or

$$L_0 = \frac{1}{\beta} \tan^{-1}\left(j\frac{Y_{tot}}{Y_0} \right). \tag{4.10}$$

This is the initial value of the length of the stub L_0 which is a function of Y_{tot}. The length of this stub depends on the length of matching lines ℓ and d.

The parameter sweep in CST was used to fine-tune the value of L_0. Figure 63 shows the CST model of the circuit with one terminal of the dipole connected to a 50 Ω line and the other diode open, to simulate a nonconducting half cycle. Figure 64 shows the best match at 10 GHz obtained with the parameter sweep. The value of L_0 is 4.226 mm, which was used in the final design. The radiation pattern for the circuit of Figure 63 is shown in Figure 65.
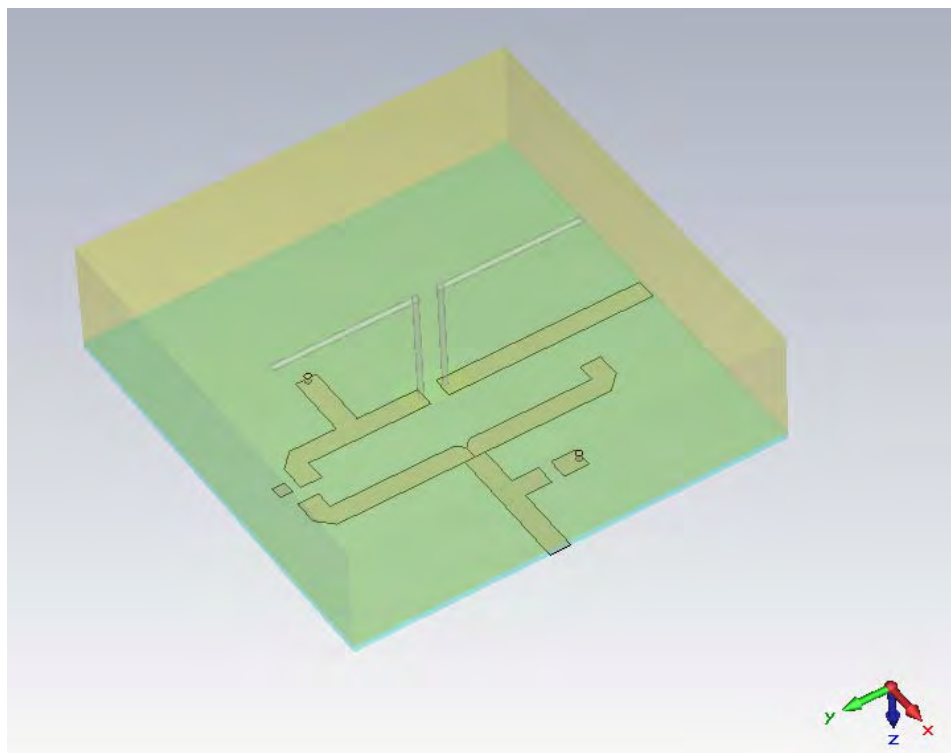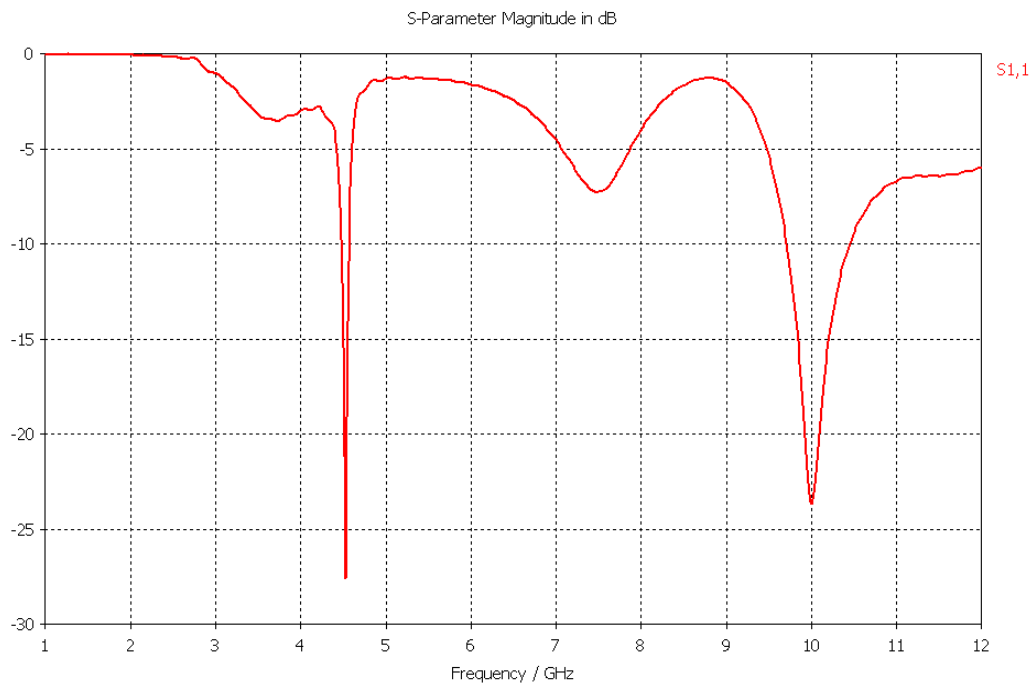
Figure 63.   CST model of the circuit.

Figure 64. S_{11} frequency response of full-wave rectenna using CST.
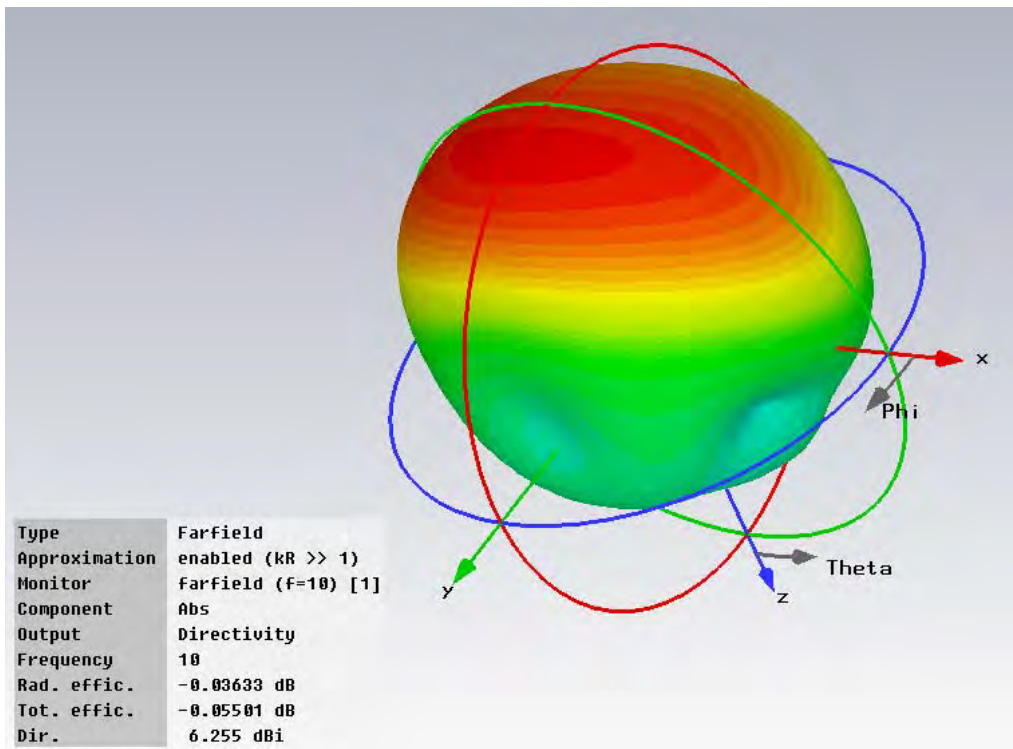
Figure 65.   Simulated result of the far-field radiation of full-wave rectenna using CST.

THIS PAGE INTENTIONALLY LEFT BLANK

V. SUMMARY, CONCLUSIONS AND RECOMMENDATIONS

A. SUMMARY

This thesis evaluated different rectenna designs for wireless power transmission for MAV applications using the ADS simulation software. The first and second chapters covered the history of WPT and research performed previously at NPS. Various rectification circuit designs and antennas were simulated using Agilent ADS software and CST Microwave Studio. A shorted stub microstrip tuner was introduced for impedance matching. The dipole-antenna array was selected to reduce the weight of the rectenna in order to hover a MAV.

A full-wave rectenna without low-pass filter was selected to reduce the weight of the rectenna element yet achieve high conversion efficiency. In addition, a harmonic balance analysis was conducted in order to compare the influence of the harmonics on various circuit designs. The full-wave rectenna circuit was simulated to verify performance, and the conversion efficiency is about 65%. The length of matching units were calculated and optimized in Microwave Studio in order to lay out the circuit.

B. RECOMMENDATIONS

The result of this thesis shows that the improved full-wave rectanna converts more dc power than a half-wave rectenna, as verified by simulation. A dipole antenna was used instead of a circular-patch antenna in order to reduce the weight of the rectenna system. The conversion efficiency of the rectenna can be improved, however, and some recommendations follow.

1. Using High-Power Transmitter and High-Gain Antenna

The performance of the WPT can be further enhanced by complementing it with a high-power transmitter and high-gain antenna to increase the power-density incident on the rectenna array.

2. Building a Hardware Prototype

Upon the successful design of the dipole antenna and rectifier circuit using CST Microwave Studio, it is necessary to build a prototype of the full-wave rectenna to measure the output dc voltage and current and determine the realized efficiency.

3. Running Simulations for an Array

The MWS simulation should be done for an array of dipoles to assess the effect of mutual coupling. The array element may need to be returned to compensate for the mutual coupling.

4. Reducing Polarization Loss

The dipole is linearly polarized, and therefore loss of signal will occur if the MAV antenna is orientated in a cross-polarized direction in flight. A circularly polarized antenna should be considered to reduce the polarization loss factor.

LIST OF REFERENCES

[1]   W. C. Brown, "The History of Power Transmission by Radio Waves," *IEEE Transactions on Microwave Theory and Techniques*, Vol. MTT-32, No. 9, September 1984.

[2]   J. J. Schlesak, Adrian Alden and Tom Ohno, "A Microwave Powered High Altitude Platform," *IEEE MTT-S Digest*, 1988.

[3]   M. Mecham, "California's PG&E links with startup on 200-megawatt SSP initiative," *Aviation Week & Space Technology*, April 2009.

[4]   S. V. Georgakopoulos and S. Jiang, "Wireless Powering of Sensors Embedded in Concrete," *Wireless and Microwave Technology IEEE 11th Annual Conference*, 2010.

[5]   U. Olgun, C.-C.Chen and J. L. Volakis, "Investigation of Rectenna Array Configurations for Enhanced RF Power Harvesting," *IEEE Antennas and Wireless Propagation Letters*, vol. 10, no. 1, pp. 262–265, April 2011.

[6]   M. T. L. Meng, "Efficient Rectenna Design for Wireless Power Transmission For MAV application," Naval Postgraduate School, December 2005.

[7]   L. H. Toh, "A Follow-up Study on Wireless Power Transmission for Unmanned Air Vehicles," Naval Postgraduate School, December 2007.

[8]   G. Tsolis, "Theoretical and experimental study of micro air vehicle powered by RF Signal at 10 GHz," Naval Postgraduate School, December 2003.

[9]   W. C. Brown, "Description and operating characteristics of the platinotron – A new microwave tub device," *Proc. IRE*, vol. 45, no. 9, pp.1209–1222, September 1957.

[10]   G. Goubau and F. Schwering, "On the guided propagation of electromagnetic wave beams," *IRE Transactions on Antenna Propagation*, vol. AP-9, pp.248–256, May 1961.

[11]   D.-G.Youn, Y.-H. Park, K.-H. Kim and Y.-C. Rhee, "A Study on the Fundamental Transmission Experiment for Wireless Power Transmission System," 1999 *IEEE TENCON*.

[12]   J. A. Hagerty, F. B. Helmbrecht, W. H. McCalpin, R. Zane and Z. B. Popovic, "Recycling Ambient Microwave Energy With Broad-Band Rectenna Arrays," *IEEE Transactions on Microwave Theory and Techniques*, vol. 52, no. 3, pp.1014–1024, March 2004.

[13]   J. O. McSpadden and J. C. Mankins, "Space Solar Power Programs and Microwave Wireless Power Transmission Technology" *IEEE Microwave Magazine*, December 2002.

[14]   A.goel, R.P. Jamdagni, and N. K. Mishra, "New Hope for Clean Energy through Exploring Space," Recent Advances in Space Technology Services and Climate Change, pp 87–89, November 2010.

[15]   Y.-H. Suh and K. Chang, "A High-Efficiency Dual-Frequency Rectenna for 2.45- and 5.8-GHz Wireless Power Transmission," *IEEE Transactions on Microwave Theory and Techniques*, vol. 50, no. 7, pp.1784–1789, July 2002.

[16]   B. Strassner, S. Kokel and K. Chang, "5.8 GHz Circularly Polarized Low Incident Power Density Rectenna Design and Array Implementation," *IEEE Antennas and Propagation Society International Symposium*, vol. 3, pp.950–953, June 2003.

[17]   J.-Y. Park, S.-M. Han and T. Itoh, "A Rectenna Design With Harmonic-Rejecting Circular-Sector Antenna," *IEEE Antennas and Wireless Propagation Letters*, vol. 3, no. 1, pp.52–54, December 2004.

[18]   J. Zbitou, M. Latrach and S. Toutain, "Hybrid Rectenna and Monolithic Integrated Zero-Bias Microwave Rectifier," *IEEE Transaction on Microwave Theory and Techniques*, vol. 54, no. 1, pp.147–152, January 2006.

[19]   T. Yamamoto, K. Fujimori, M. Sanagi and S. Nogi, "The Design of mw-Class RF-DC Conversion Circuit using the Full-Wave Rectification," The 37th European Microwave Conference, Proceeding, 9–12 October 2007, pp.905–908.

[20]   U. Olgun, C.-C. Chen and J. L. Volakis, "Low-profile Planar Rectenna for Batteryless RFID Sensors," *IEEE Antennas and Propagation Society International Symposium*, pp.1–4, July 2010.

[21]   R. L. Vitale, "Design and Prototype Development of a Wireless Power Transmission System For a Micro Air Vehicle (MAV)," Naval Postgraduate School, June 1999.

[22]   T.-W. Yoo and K. Chang, "Theoretical and Experimental Development of 10 and 35 GHz Rectennas," *IEEE Transactions on Microwave Theory and Techniques*, vol. 40, no. 6, pp.1259–1266, June 1992.

[23]   H.-K. Chiou and I.-S. Chen, "High-Efficiency Dual-Band On-chip Rectenna for 35- and 94-GHz Wireless Power Transmission in 0.13-μm CMOS Technology," *IEEE Transactions on Microwave Theory and Techniques*, vol. 58, no. 12, pp. 3598–3606, December 2010.

[24]   F. T. Ulaby, *Fundamentals of Applied Electromagnetics*, pp.88–92, Prentice Hall, Person Education Inc, 2004.

INITIAL DISTRIBUTION LIST

1. Defense Technical Information Center
   Ft. Belvoir, Virginia

2. Dudley Know Library
   Naval Postgraduate School
   Monterey, California

3. Dan C. Boger
   Chairman, Information Science Department
   Naval Postgraduate School
   Monterey, California

4. Professor David C. Jenn
   Professor, Department of Electrical & Computer Engineering
   Naval Postgraduate School
   Monterey, California

5. Professor Ric Romero
   Assistant Professor, Department of Electrical & Computer Engineering
   Naval Postgraduate School
   Monterey, California

6. Robert D. Broadston
   Staff, Department of Electrical & Computer Engineering
   Naval Postgraduate School
   Monterey, California

7. Chun-Yi Liu
   Department of Electronic Warfare Systems Engineering
   Naval Postgraduate School
   Monterey, California

8. Deanna Y. Tyler
   US Army CERDEC, C2D
   Aberdeen, Maryland